



HAL
open science

Paleoceanography of the Strait of Hormoz and its link to paleoclimate changes since the mid-Holocene

Mohammad Ali Hamzeh, Maziar Khosravi, Xavier Carton, Dariush Yarahmadi, Ezatollah Safarkhani

► **To cite this version:**

Mohammad Ali Hamzeh, Maziar Khosravi, Xavier Carton, Dariush Yarahmadi, Ezatollah Safarkhani. Paleoceanography of the Strait of Hormoz and its link to paleoclimate changes since the mid-Holocene. CONTINENTAL SHELF RESEARCH, 2021, 226, 10.1016/j.csr.2021.104507 . insu-03683257

HAL Id: insu-03683257

<https://insu.hal.science/insu-03683257>

Submitted on 14 Apr 2023

HAL is a multi-disciplinary open access archive for the deposit and dissemination of scientific research documents, whether they are published or not. The documents may come from teaching and research institutions in France or abroad, or from public or private research centers.

L'archive ouverte pluridisciplinaire **HAL**, est destinée au dépôt et à la diffusion de documents scientifiques de niveau recherche, publiés ou non, émanant des établissements d'enseignement et de recherche français ou étrangers, des laboratoires publics ou privés.

Paleoceanography of the Strait of Hormoz and its link to paleoclimate changes since the mid-Holocene

Hamzeh Mohammad Ali ^{1,*}, Khosravi Maziar ¹, Carton Xavier ², Yarahmadi Dariush ³,
Safarkhani Ezatollah ³

¹ Iranian National Institute for Oceanography and Atmospheric Science (INIOAS), No.3, Etemad Zadeh St., Fatemi Ave., Tehran, IR, Iran

² Laboratory for Ocean Physics and Satellite Remote Sensing (LOPS), UMR6523, Ifremer, Univ. Brest, CNRS, IRD, Brest, France

³ Department of Geography, Faculty of Literature and Humanities, Lorestan University, Khorramabad, Iran

* Corresponding author : Mohammad Ali Hamzeh, email address : Hamzeh@inio.ac.ir

Abstract :

This paper presents the paleocurrent evolution of the Persian Gulf deep water (PGDW) during the last 5000 years using faunal (foraminiferal assemblage) and non-faunal (magnetic susceptibility, sediment grain size, number of coarse relict particles and physicochemical characteristics) indicators from a 133 cm long core retrieved from the Strait of Hormoz (SH). Our results suggest that the precession-related insolation change and solar variability induced long-term and short-term sea surface temperature (SST) rise and fall resulted in variation of PGDW outflow strength. Two periods of decreasing SST (5000–4300 and 2000–1450 cal yr BP), accompanied by wetter conditions in the Middle East, are related to the reduction of the PGDW current velocity. A combination of high sedimentation rate (0.72 mm yr⁻¹, due to high terrigenous input) with a relatively low bottom flow energy cause the settling of finer sediments providing a favourable environment for the expansion of benthic foraminifera (dominated by infaunal taxa). On the contrary, the PGDW current velocity strengthens in the periods of SST increase (4300–2000 and 1450 cal yr BP to present) with decreasing sedimentation rate (0.15–0.34 mm yr⁻¹, due to low river discharge). During both periods of high-velocity bottom currents, the benthic foraminifera accumulation rate decreases. However, as the PGDW brings a relatively high amount of dissolved oxygen (3.25 mg/l in summer and 4.79 mg/l in winter) and phytodetritus particles, compared to the surrounding water, some particular foraminifera (especially robust suspension feeder epifaunal taxa) evolved. SST increase, intensified by anthropically caused global warming, may lead to PGDW intensification in the future.

Highlights

► Since the mid-Holocene, PGDW intensity has been under influence of the continental climate of SW Asia and the Arabian Sea SST. ► SST intensification (4500 to 3000 and 1400 cal yr BP to present), causes increasing bottom current energy of the Strait of Hormoz and decreasing river discharges. ► Although high energy bottom currents provide a hostile environment for the benthic fauna, it brings high DO content bottom waters.

Keywords : Benthic foraminifera, Persian Gulf deep water, Relict sediments, SST, Terrigenous input

34 1. Introduction

35 The Strait of Hormoz (SH), also called Strait of Hormuz, is a well-known 55 to 95 km wide
36 channel linking the Persian Gulf (PG) with the Gulf of Oman and the Arabian Sea, and also,
37 separates Iran (in the north) from the Arabian Peninsula (in the south). This waterway is of
38 great strategic and economic importance, especially as about one-fifth of the world's oil supply
39 and one-third of liquefied natural gas collected from various ports on the PG passes through
40 the strait (Sheppard et al. 2010). On the other hand, SH bottom is the passageway of the Persian
41 Gulf deep water (PGDW) (Johns et al. 2003). This strait plays a critical role in determining the
42 circulation in the PG by constricting the water exchange between the PG and the open ocean.
43 The PGDW outflow descends across the shelf in the northern Gulf of Oman, entrains ambient
44 fresher water and is intensively diluted (Wyrski 1971). Undoubtedly, climate change plays a
45 fundamental role in determining the outflow regime by altering the contrast in physical
46 properties of two water bodies separated by the SH (Yao and Johns 2010; Bower et al. 2000).

47 Lying at the transition zone between the Mediterranean winter rain (whose route is
48 controlled by Mid Latitude Westerlies (MLW)) and the Indian Summer Monsoon (ISM)
49 domains, the SH has experienced various climatic regimes during the Holocene (Regard et al.
50 2006; Arz et al. 2003). The relative influence of the above components of atmospheric
51 circulation patterns is dependent on variations in the mean latitudinal position of the Inter-
52 Tropical Convergence Zone (ITCZ) (Kodera 2004). Since the mid-Holocene, precession and
53 obliquity cycles caused a shift of perihelion from September to January and a decrease in the
54 tilt of the Earth's axis. The resulting radiative changes caused a decrease in the summer and an
55 increase in the winter insolation in the northern hemisphere (Lorenz et al. 2006; Kim et al.
56 2004). These seasonality changes in insolation caused the southward migration of ITCZ being
57 accompanied by significant paleoclimate variations in different parts of SW Asia particularly
58 the study area which is located within this translocation territory (Hamzeh et al. 2016;
59 Fleitmann et al. 2007). Besides, the shallowness of this area makes its response to
60 meteorological variables quick and dramatic (Hunter, 1986). The SH is thus an essential region
61 for the study of the interactions between climatic changes and their effects on
62 paleoceanography. Although continuous Holocene climate records from the Mediterranean and
63 ISM-dominated areas allow comparing the regional climate with global climatic signals, the
64 interaction of paleoclimate changes and paleoceanography of the PG and SH has remained
65 unknown.

66 Paleocceanography studies reveal that high-energy bottom currents have strong effects
67 on, for instance, water turbulence, suspension load, and boundary layers, which should
68 significantly influence the sedimentology and ecological conditions at the seafloor (Zhong et
69 al. 2017; Shimmield et al. 1994). These currents can be traced by evaluating the physical and
70 ecological characteristics of bottom sediments (Schönfeld 1997; Hollister and Heezen 1972).
71 In the absence of current measurements, some proxies such as grain size analysis and benthic
72 foraminiferal assemblages could be used to estimate paleo-current variations (Schönfeld
73 2002a, 2002b; Hollister and Heezen 1972). Lutze and Altenbach (1988) showed that intensified
74 bottom water currents influence the physical properties of microhabitats and composition of
75 the benthic foraminiferal fauna as well. Studies of particle size also shed light on many facets
76 of sea bottom depositional conditions such as relative bottom current speed (McCave 2007).
77 In the present paper, the influence of paleoclimate on paleocurrent change of deep outflow
78 regime in the PG and SH is evaluated by using physical characteristics and benthic
79 foraminiferal assemblages of bottom sediments.

80

81 **2. Materials and Methods**

82 **2.1. Strait of Hormoz**

83 The strategically and economically pivotal SH connects the PG to the continental shelf in the
84 northwestern Gulf of Oman. It is 56 km wide at its narrowest point (although its central channel
85 is about half as wide) with a sill depth of 80 m (Kassler 1973). Geologically, the study area
86 corresponds to the transition zone between the subduction (the Indian Ocean vs Eurasian plates)
87 and collision (Arabian vs Eurasian plates) zones (Regard et al. 2006). The geology of the area
88 exhibits the easternmost folds of the Zagros fold-thrust belt. The anticlines of the coastal area
89 are capped most often by Eocene to Miocene limestone rocks, while the synclines are
90 composed mainly of Miocene sandstone and marls as well as Plio-Pleistocene conglomerates
91 (Molinari et al. 2004). To the east, the structures of the Zagros Mountains suddenly change to
92 the NNW-trending folds and thrusts of the Zendan–Minab Belt composed of a poorly
93 consolidated Mio-Pliocene pebbly sandstone and marls (Molinari et al. 2004).

94 SH contains the islands of Qeshm, Hormoz (Hormuz), Lārak and Hengām. Qeshm, the
95 largest island of the PG, forms the northern flank of the SH and southeastern marginal foreland
96 of the ZFTB (Fig. 1). Numerous salt diapirs containing Lower Cambrian volcano-sedimentary
97 complex (basalt, basaltic andesite, andesite, trachyte, pyroclastics, evaporite rocks and

98 Precambrian sedimentary units) occur on the mainland also in the form of small islands in the
99 PG (Taghipour and Taghipour 2009). Kuh-e-Namakdan (Mt. Saltcellar) is an instance of a salt
100 dome being exposed in the western part of Qeshm Island (Haghipour and Fontugne 1993).
101 During the last glacial maximum (when sea level was 120 m lower than today) until about
102 14000 yr BP, the entire area was a dry valley and reached its present water level about 6000
103 years B.P. Based on the Holocene paleoshoreline reconstruction models, the coring area was
104 inundated about 8000 yr BP (Bruthans et al. 2006; Pirazzoli et al. 2004).

105 Modern bottom sediments of the PG are mostly composed of terrigenous sand
106 components, relict sand particles and biogenic carbonates and, especially at the deeper parts,
107 are characterized by sandy silt (sand content: 20 - 30%). At the bottom of the main channel,
108 gravelly sand, gravelly sand and muddy sandy gravel appear. Pebble fraction in some areas
109 reaches to more than and 30% (Hamzeh in press).

110 Freshwater inflow is dominated by the northern coasts (originating from Taurus and
111 Zagros Mountains). The annual mean flow of the rivers decreases from NW to SE and is as
112 follow: Karoon: 20, Karkheh: 5.5, Hendijan: 2, Jarrahi and Mond: 1.5, Helleh: 0.6, Mehran and
113 Kol: 0.1 km³ yr (Al-Said et al. 2018).

114

115 **2.1.1. Climate and paleoclimate**

116 Coastal regions of SH receive Mediterranean-type winter precipitation, in association with
117 MLW. Because of the influence of the Siberian High, only deep depressions from the
118 Mediterranean coast can get to the coastal area. In this area, the absence of significant
119 topographic barriers along the MLW allows Atlantic low-pressure cells to penetrate. The warm
120 surface waters of the PG provide subsidiary moisture sources allowing storms to maintain or
121 reinforce as they move to the eastern PG and SH (Regard et al. 2006). During the last half-
122 century, mean annual precipitation and mean annual air temperature the area have been about
123 180 mm and 27 °C respectively (IWRMC, 2016). During the summer, the moist MLW moves
124 northward and hot and dry weather prevails. Due to low pressures over southern Asia, the
125 prevailing winds are thus northerly and northwesterly (such as the dominant northwesterly
126 wind known as “Shamal” which enhances dust phenomena particularly in summer months) and
127 the ITCZ lies at its northernmost position (the extreme south of Iran). However, the SH region
128 remains beyond the influence of Indian monsoon (Fig. 1) (Regard et al. 2006). Below the ITCZ,
129 prevailing winds are westerly and southwesterly winds and ISM rains are dominated. The
130 Hormoz Strait area thus is the boundary between the extratropical, winter rainfall domain, and

131 the tropical, summer monsoon rainfall domain. However, it is suggested that, due to orbitally-
132 driven insolation forcing, during the early-mid Holocene, a more northern position of ITCZ
133 caused monsoon-induced summer precipitation in the study area (Fleitmann et al. 2007). Many
134 Holocene paleoclimate records suggest that environmental changes triggered a range of cultural
135 responses, from demise to reorganization, to the expansion of ancient societies in southern Iran.
136 According to these studies, Bronze Age civilizations along rivers in southern Iran such as Tape
137 Yahya and Konar Sandal (Majidzadeh 2003; Potts et al. 2001) along the Halil River, Shahdad
138 (Salvatori and Vidale 1982) beside the Shahdad River and Shahr-e Sukhteh (Tosi 1983) ashore
139 Hirmand River flourished around 7 - 4 kyr BP due to mid-Holocene ISM-induced climatic
140 optimum. After this period, the southward migration of ITCZ caused relatively stronger ISM-
141 dominated rainfall gradually replaced by the weaker Mediterranean winter precipitations, and
142 consequently, the demise of the above civilizations. This can be attributed to the precessional
143 shift of perihelion from September in the middle Holocene to January today over the last 5000
144 years which caused the reduction in insolation during the summer season in the Northern
145 Hemisphere. At the same time, insolation increased during winter on almost the whole Earth
146 (Rimbu et al. 2004). Therefore, the SH is a remarkable environment to assess the orbitally-
147 induced temperature and wind regime changes as well as the proportions of various
148 atmospheric systems affecting the paleoceanography and hydro-climatic regime of the area.

149

150 **2.1.2. PG circulation and water exchange through the SH**

151 As a semi-enclosed continental shelf sea, the PG exhibits many results of SST and wind
152 intensity changes, as well as constricted water exchange with the open ocean. The region
153 comprised of the PG, SH, and the Gulf of Oman is submitted to a strong solar heat flux, which
154 leads to substantial evaporation (approximately 1.5 m yr^{-1}). In the PG basin, from April to July
155 a barotropic cyclonic gyre governs the general circulation. Due to the winter cooling, and under
156 influence of wind forcing (leading to a decrease in stratification), this pattern breaks down into
157 smaller features (Pous et al. 2015). Evaporation (proportional to the ocean-atmosphere
158 temperature difference and the wind velocity) leads to the formation of a warm and salty
159 (dense) water mass in the PG called PGDW (Persian Gulf Deep Water) which is one of the
160 most saline water masses in the world ocean (Reynolds, 1993). PGDW is formed at two
161 locations including: a) the northwestern part of the PG, along the Kuwait and the Saudi Arabia
162 shallow coasts, and b) over the southern banks (Arabian shallow shelf) (Fig. 1b); at both places,

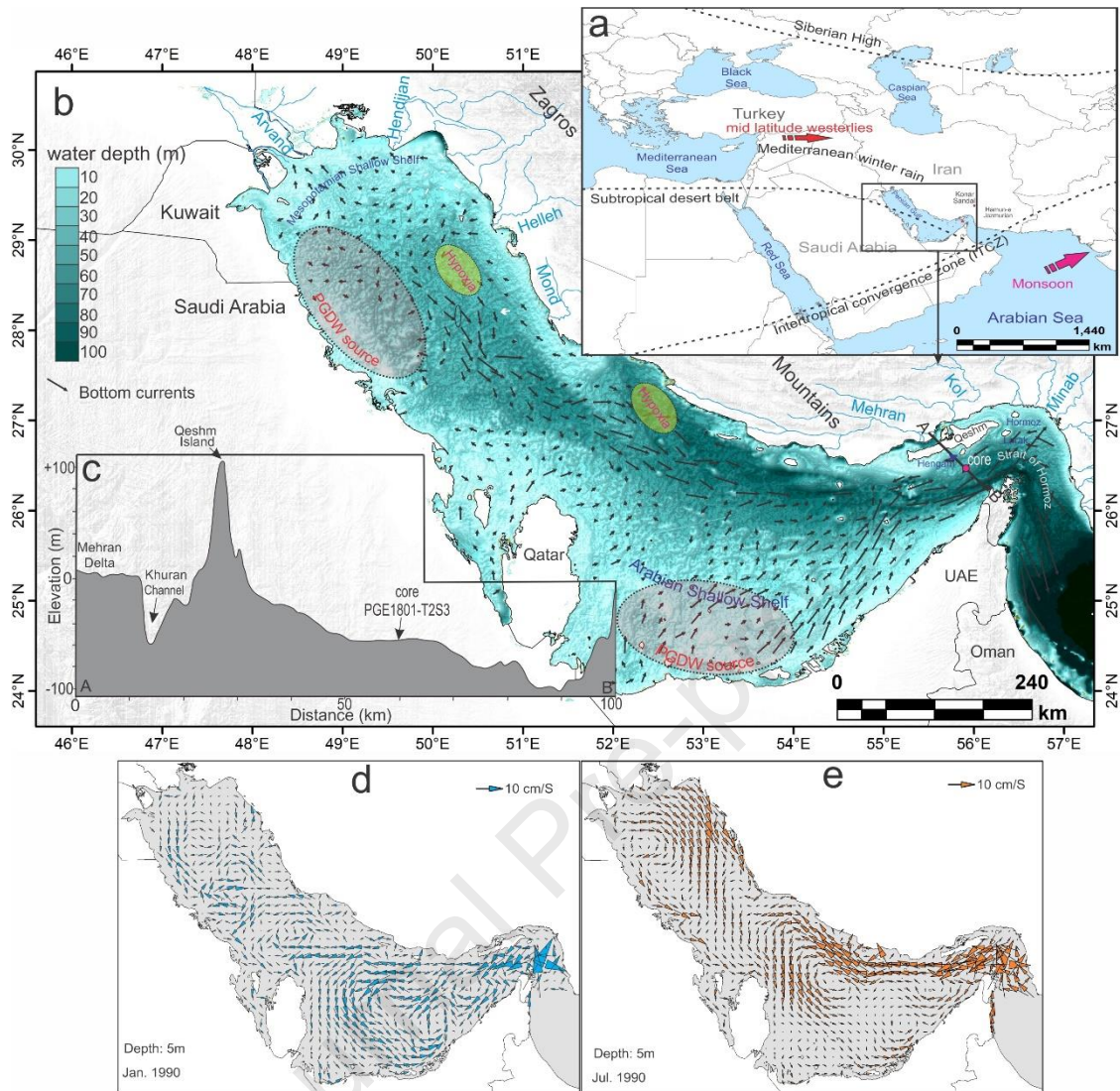
163 the deep water masses are formed during fall and winter (Yao and Johns 2010; Lorenz et al.
164 2020). Due to their different distance to the SH, the first and the second water masses reach the
165 SH during summer-early fall and late winter-spring respectively. A permanent southeastward
166 deep current advects the dense water from the northwest towards the SH year-round, while
167 dense water formed in the southern banks can flow to the SH by November to April. However,
168 some minor sources of PGDW are located in central parts of the PG basin all year round (Pous
169 et al. 2015). The maximum transport occurs in July with a value of $150.000 \text{ m}^3 \text{ s}^{-1}$, while the
170 minimum transport ($70.000 \text{ m}^3 \text{ s}^{-1}$) occurs in January (Johns et al. 2003). The PGDW is flushed
171 out of the PG through the SH (Johns et al. 2003) and then stabilizes at depths of 250-350 m in
172 the Gulf of Oman. It spreads first along the Omani coast (Bower et al. 2000) and forms coastal
173 undercurrents.

174 The PGDW leaving the PG near the bottom of the SH is compensated by the surface
175 inflow of Indian Ocean Surface Water (IOSW) (Johns et al. 2003, Yao and Johns 2010). All
176 year round, an inflow of low-salinity IOSW enters the PG, on the Iranian side of the SH. Then,
177 under the influence of the Coriolis force, it is deflected to the North (along the Iranian coast)
178 and it forms a basin-wide cyclonic circulation in the southern PG (Fig. 1b). It is worth
179 mentioning that at the SH, the IOSW bifurcates and that a large volume of water enters the PG
180 south of the Qeshm Island, while the rest enters the PG through the Khuran Channel, a tidal
181 channel located north of the Qeshm Island (Khosravi et al. 2018).

182 The inter-annual variability of the PG average salinity is significant, and it dominates the
183 seasonal variability. These long-term variations are more related to the water exchange at SH
184 than to atmospheric fluxes. These water exchanges at the strait play an essential role in the PG
185 salt budget. The inter-annual variations of the circulation due to the variations in (E-P)
186 significantly impact the net transport at SH. This circulation is driven by various mechanisms
187 (density gradients and wind stress), and by their nonlinear interactions (Pous et al. 2015).

188 The IOSW inflow exhibits a significant seasonal variability. The volume flux of IOSW
189 at SH is $7250 \text{ km}^3 \text{ yr}^{-1}$ (Sheppard et al. 2010) and it is weaker (about 10 cm/sec) in spring and
190 autumn and stronger (about 20 cm/sec) in summer (Hunter 1986) suggesting an increased
191 transport of IOSW to the northwestern PG. The salinity of the outflow has a mean value of 39.3
192 psu with considerable intra-seasonal variability (ranging from 39.5 to 40.8 psu). The PGDW
193 volume flux at SH is $6620 \text{ km}^3 \text{ yr}^{-1}$ (Shepard et al. 2010).

194



195

196

197 **Fig. 1.** a) General map of the Middle East containing the modern climatic setting including the boundary

198 between the Mediterranean winter rain domain and the subtropical desert belt (after Arz et al. 2003), the position

199 of the ITCZ (Regard et al. 1997) and Siberian High (Mayewski et al. 1997). b) The PG and SH and dominant

200 bottom currents (Pous et al. 2015). c) Depth transect (A-B) perpendicular to the SH axis showing the coring

201 location. d) surface currents in winter and e) summer (Pous et al. 2015).

202

203 At the SH, the vertical structure of the flow is a two-layer exchange in winter; the

204 surface inflow has a salinity lower than 38.5 psu in the northern part of the SH; the deep outflow

205 has a temperature of about 24°C and salinity of 40.5 psu. The deep outflow and the surface

206 inflow speeds in winter are about 10 cm/s. In summer and fall, in addition to the upper inflow

207 of IOSW and of the deep outflow, the warm and salty waters from the northwestern and

208 southern banks feed an outflow at intermediate depths (between 10 and 40 m) in the southern

209 part of the strait. The temperature and salinity of the outflow water are < 27 °C and >40.5 psu

209 respectively, with a maximum velocity of 20 cm/s (Johns et al. 2003).

210

211 **2.2. Coring and relevant analyses**

212 The data of this study are the result of analyzing a 133 cm long sediment core PGE1801-T2S3
213 (hereafter called T2S3) retrieved during the Persian Gulf Explorer (PGE) cruise in January
214 2018 (PGE1801). The core was taken at the depth of 56 m west of Strait of Hormoz (15 km,
215 south of Hengām Island (lat: 26.464833, long: 55.914841)) by a gravity corer with a 5 cm
216 diameter (Fig. 1). Although the core was retrieved from the edge of the deep central channel of
217 the SH, however, it lies below the depth of the PGDW outflow domain, at least during summer
218 (Azizpour et al. 2014). Dissolved Oxygen (DO) and salinity of water samples taken from the
219 surface, 5 m depth and bottom in this cruise (winter 2018) and cruise PGE1803 (summer 2018)
220 were measured by a Hach multimeter. In the laboratory, an MS2C Bartington magnetic
221 susceptibility meter was used for whole-core Magnetic Susceptibility (MS) measurements at 1
222 cm increments. Then, the core was cut along the longitudinal axis and one half-core used for
223 reconstruction of the SST of the PG (Safarkhani et al. 2021) and another half-core used for this
224 study. Initially, the preliminary studies including the imaging and the accurate description of
225 sedimentological observations and sedimentary structures were done. Fifty-three subsamples
226 were taken at 2.5 cm intervals (each sample covers ~35-165 years depending on the sample
227 depth (Fig. 2)). 10 cm³ from wet sediment was taken using the syringe technique to determine
228 physical properties of sediment including water content, porosity and wet bulk density
229 (Mudroch et al. 1997). Total Organic Matter and carbonate per cent were measured using the
230 loss-of-ignition (450 °C, 5 h) and acid dissolution methods (hydrochloric, 1N), respectively
231 (Heiri et al. 2001; Mudroch et al. 1997). Sand and mud fractions were separated by wet sieving
232 (using 63 µm sieving). A FRITSCH laser particle sizer was used to separate silt and clay
233 fractions as well (Konert and Vandenberghe, 1997). >250 µm fraction from a 10 cm³ sediment
234 samples was used for counting relict particles under Nikon stereomicroscope (Sarnthein 1971).
235 Finally, the >63 µm fraction was used to obtain census data of benthic foraminiferal
236 assemblages. The foraminiferal taxa were identified by Haynes (1981) and Loeblich and
237 Tappan (1988) textbooks and previous studies of the area (Amao et al. 2018; Saidova 2010).
238 At least 300 individuals were counted to determine the relative abundance of species to
239 characterize an assemblage (Murray, 2006). Benthic foraminiferal accumulation rate (BFAR)

240 (number of specimens/cm² 10 yr⁻¹) were measure based on Herguera (1992). All frequency and
 241 abundance of benthic foraminifers are reported per 10 cm³ of sediment.

242

243 **2.3. Radiocarbon dating**

244 After evaluating the physical properties of the core sediments (especially MS), three sediment
 245 samples were taken from depths of 50, 90 and 120 cm (Table 1, Fig. 2), where significant
 246 changes happen (Fig. 3). As the organic remains contained in bulk sediments may originate
 247 from numerous sources of different ¹⁴C ages, thus yielding inaccurate ages, we collected
 248 benthic foraminiferal tests (*Ammonia beccarii*; Linnaeus, 1758) to obtain more precise dating
 249 results (Olsen et al. 2017). *A. beccarii* tests with the size range of 300 to 500 µm were picked
 250 and sent to the Poznan laboratory to determine the age by AMS radiocarbon method and
 251 calibrated using Marine20 (Reimer et al. 2020) regarding the value proposed as the reservoir
 252 effect for the PG and the Arabian Sea ($\Delta R = 190 \pm 25$; Southon et al. 2002). The ages were
 253 reported based on the mean probability of error 2 σ (Table 1). Age-depth relationship of core
 254 T2S3 produced by CLAM software (Blaauw 2010). All ages mentioned in this study are
 255 reported as the year before the present time (cal yr BP) and thousands of years before the
 256 present time (cal kyr BP).

257

258 **Table 1.** Radiocarbon age report for three benthic foraminifera samples from the core T2S3. ¹⁴C ages were
 259 calibrated based on Marine 13 calibration dataset.

Sample number	Laboratory number	Sample material	Number of tests	Sample weight (g)	Depth (cm)	Age (2 σ \pm) (yr BP)	Calibrated age range (cal yr BP)
TS-50	Poz-107160	<i>A. beccarii</i>	278	0.049	50	2120 \pm 30	1370-1580
TS-90	Poz-107161	<i>A. beccarii</i>	183	0.039	90	2595 \pm 30	1921-2144
TS-120	Poz-107162	<i>A. beccarii</i>	251	0.058	120	4420 \pm 30	4195-4439

260

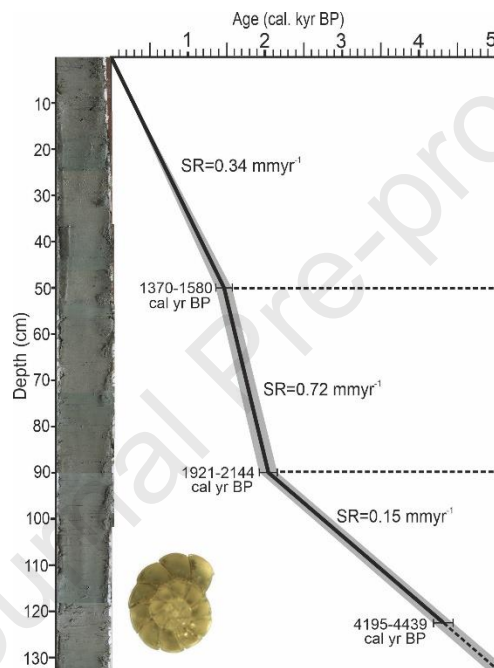
261 **3. Results**

262 **3.1. Age-depth model**

263 Figure 2 shows the age-depth diagram of the core based on three age-determined samples
 264 considering the zero time for surface sediments. In this way, the line of changes in the core age

265 was plotted between four horizons of zero, 50, 90 and 120 cm. Since the characteristics of
 266 sediment material of deeper than 120 cm (the lowest age-determined sample) do not show
 267 significant changes, the age-depth diagram in the end part is extended to the end (bottom 13
 268 cm) without changing the slope. As such, the age determination diagram is plotted assuming
 269 that the sedimentation rate (SR) is uniform between the age-determined horizons (Figure 2).

270 The highest SR (0.72 mm yr^{-1}) is observed in the middle parts of the core (depth 50-90
 271 cm), while the lower depths represent the lowest (0.15 mm yr^{-1}). With an SR of 0.34 mm yr^{-1} ,
 272 the topmost section lies in between. The overall SR of the core T2S3 is in agreement with the
 273 findings of Al-Ghadban et al. (1998) in the SH.



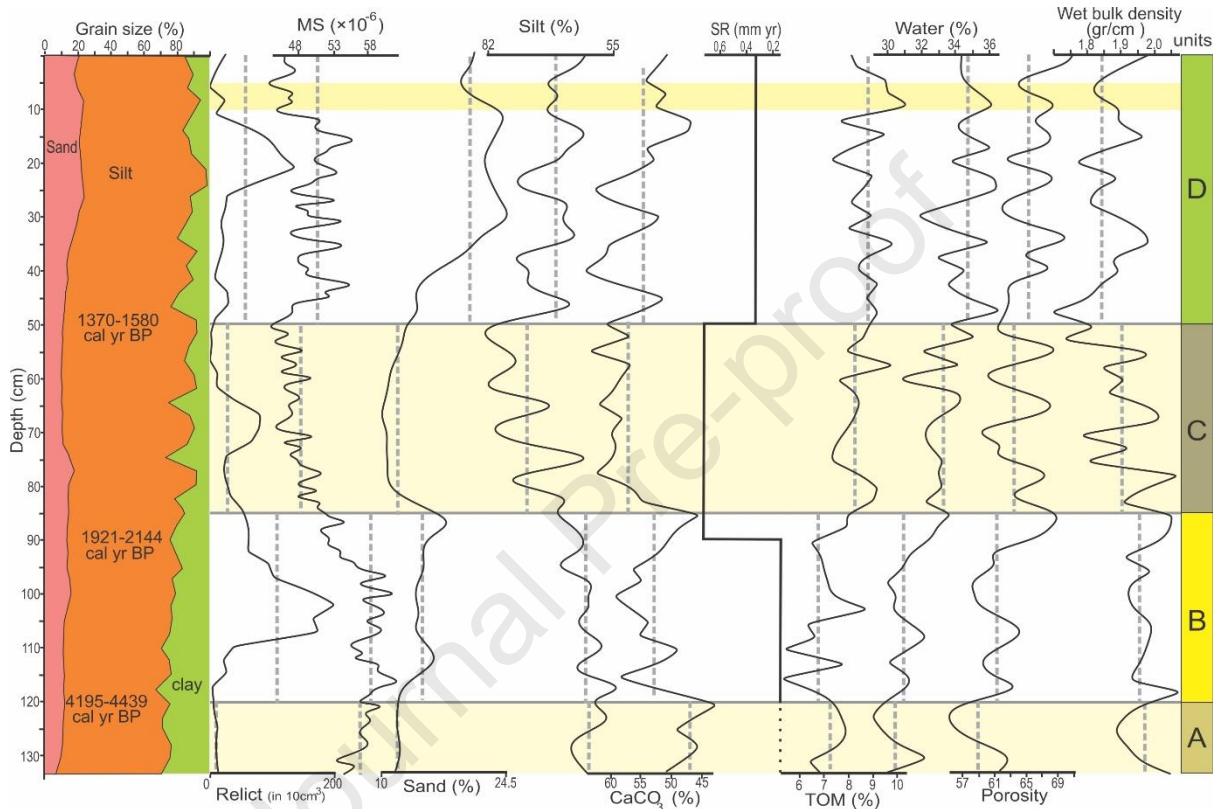
274
 275 **Figure2.** Age-depth diagram of core T2S3 from three age-determined samples. The Grey bars show 95%
 276 confidence intervals. The image of the age-determined foraminifera (*A. beccarii*) is shown at the bottom of the
 277 figure.

278

279 3.2. Dissolved oxygen and salinity of the water column

280 The characteristics of the water column at the SH shows that, during summer when the water
 281 layers are distinctly formed and PGDW is strengthened, DO differences between the surface
 282 (6.44 mg/l) and bottom (3.25 mg/l) are relatively high. However, at the same time, hypoxic
 283 conditions ($\text{DO} < 1 \text{ mg/l}$) prevail at some areas deeper than 50 m in the central and western
 284 basins of the PG (Fig. 1d) which are not located on the path of PGDW (Saleh et al. in press).
 285 PGDW salinity at this time is 40.8 psu as well. In winter, DO concentrations at the surface,

286 depth 25 m and bottom (depth 56 m) are 5.61, 5.43 and 4.79 mg/l respectively. Bottom salinity
 287 during winter is 39.0 psu which is 1.8 psu lower than that of summer. This slight difference
 288 between the surface and bottom is attributed to the vertical mixing. This shows that the PGDW
 289 has a fundamental role to provide DO at the bottom of the SH, especially during summer when
 290 the situation in other deep areas of the PG and SH is unfavourable for benthic communities.
 291



292
 293 **Fig. 3.** Variations in sedimentological and geochemical characteristics in core T2S3. Graphs range between
 294 minimum and maximum values. Vertical dashed lines show the average values in units.

295

296 3.3. Sedimentological characteristics

297 The lithology of the core T2S3 mostly consists of pale olive (5Y 6/3) sandy silt units. Only the
 298 sediments of the bottommost sample (below 130 cm), due to falling sand content below 10%,
 299 are silt. Generally, sedimentological proxies can be classified into two groups. The first one
 300 varies somewhat steadily with depth and shows an increasing or decreasing trend upward.
 301 These parameters following post-depositional influences (i.e. compaction and degradation)
 302 include TOM, water content, porosity and wet bulk density. Due to the sediment compaction,
 303 water content and porosity of core sediments increase upward, while wet bulk density shows a
 304 reverse trend (Fig. 3, Table 2). TOM variation has a decreasing downward trend. The members

305 of the second group show more intricate variations likely due to the paleoenvironmental
 306 changes during the sedimentation. The variation trend of relict particles, MS and sand content
 307 show a slightly positive correlation. On the other hand, SR, silt content and calcium carbonate
 308 per cent variations are positively correlated. Moreover, the two above groups of proxies
 309 oscillate conversely.

310 The relict grains are a mixture of various components including mostly black ooids,
 311 faecal pellets, mollusc shell fragments, bryozoa, foraminifera as well as corals. Furthermore,
 312 light coloured terrigenous particles are also observed (Fig. 4) which are embedded in an
 313 aragonite mud matrix. Sarthein (1972) defined the palaeoenvironment of this community as a
 314 transformation of successive intertidal carbonate areas into deep water areas. He also suggests
 315 that the processes of black colouring and glauconization of grains, and the weathering on the
 316 surface of the skeletal remains most likely took place in the early, shallow water stage.

317 Altogether, based on basic sedimentological data, MS as well as foraminiferal
 318 assemblages, we have recognized four units, A, B, C and D (Fig. 3). According to Fig. 3, some
 319 abrupt changes in MS values and grain size distribution can be distinguished, which could be
 320 related to changes in sediment transportation/deposition conditions.

321

322 **Table 2.** Variations in sedimentological and geochemical characteristics in four units of core T2S3.

323

	Unit A		Unit B		Unit C		Unit D		Entire the core	
	Range	Ave.	Range	Ave.	Range	Ave.	Range	Ave.	Range	Ave.
	120-133 cm		85-120 cm		50-85 cm		0-50 cm			
	4320-5000 cal yr BP		1980-4320 cal yr BP		1470-1980 cal yr BP		0-1470 cal yr BP			
Sand (%)	8-13	11	12-18	15	10-16	11	13-24	19	8-24	15
Silt (%)	60-67	63	56-68	62	59-82	74	62-79	69	56-82	69
Clay (%)	22-29	26	16-32	23	7-26	14	2-23	12	2-32	17
MS ($\times 10^{-5}$ SI)	5.6-5.6	5.6	5.2-6.2	5.7	4.4-5.6	4.8	4.4-5.4	5.0	4.4-6.2	5.2
Relict no (in 10 cm ³)	11-18	15	9-210	101	5-87	38	5-145	45	5-210	52
CaCO ₃ (%)	43-51	47	49-59	54	50-63	58	50-64	56	43-64	55
TOM (%)	6.4-7.9	7.3	5.3-8.6	6.8	7.4-9.7	8.3	7.3-10.4	8.8	5.3-10.4	8.0
Porosity	55-63	59	58-66	61	57-70	64	60-71	65	55-71	63
Wet bulk density (gr/cm ³)	1.9-2.1	2.0	1.9-2.0	2.0	1.7-2.1	1.9	1.7-2.0	1.8	1.7-2.1	1.9

324

325 Unit A: This relatively thin basal unit represents the lowest sand (8-13 %), silt (60-67 %) and
 326 calcium carbonate (43-51 %) content of the core with an upward increasing trend. The number
 327 of relict particles is lower than that of other units, too. Conversely, the MS values are higher
 328 than in other units except for B.



329
 330 **Fig. 4.** Digital image of some relict particles including terrigenous (a-h), ooids/pellets (i-j), benthic foraminifera
 331 (k-o) as well as bivalve (p) and crustacean shells (q). some of the terrigenous particles are embedded in an
 332 aragonite cement (b).
 333

334 Unit B: MS an increasing upward trend in the former unit is continued to the base of unit B to
 335 reach the maximum values ($5.2 - 6.2 \times 10^{-5}$ SI) in this unit. Sand and CaCO_3 content increase
 336 by 15-30 % in this horizon as well. However, the most dramatic increase happens in relict
 337 particles. The number of these grains in this unit is 7 times more than that of unit A. On the
 338 other hand, silt content remains relatively unchanged and, together with unit A, are lowest in
 339 the core. These low values coincide with the lowest sedimentation rate (0.15 mm yr^{-1}).

340 Unit C: An abrupt decrease in the number of relict particles (2.6 times) separates this 40 cm
 341 long unit from the above and below ones. This decline correlates with decreasing sand content
 342 and MS values (16 and 14 % respectively) with a lower magnitude. Instead, silt (mean: 74%)
 343 and calcium carbonate (mean: 58%) content co-increase with the sedimentation rate (0.72 mm
 344 yr^{-1}) and attain their highest values in the core.

345 Unit D: This unit is characterized by a re-increasing number of relict particles, MS values and
 346 sand content. The magnitude of these variations for relicts and MS (18 and 4 %) is lesser than

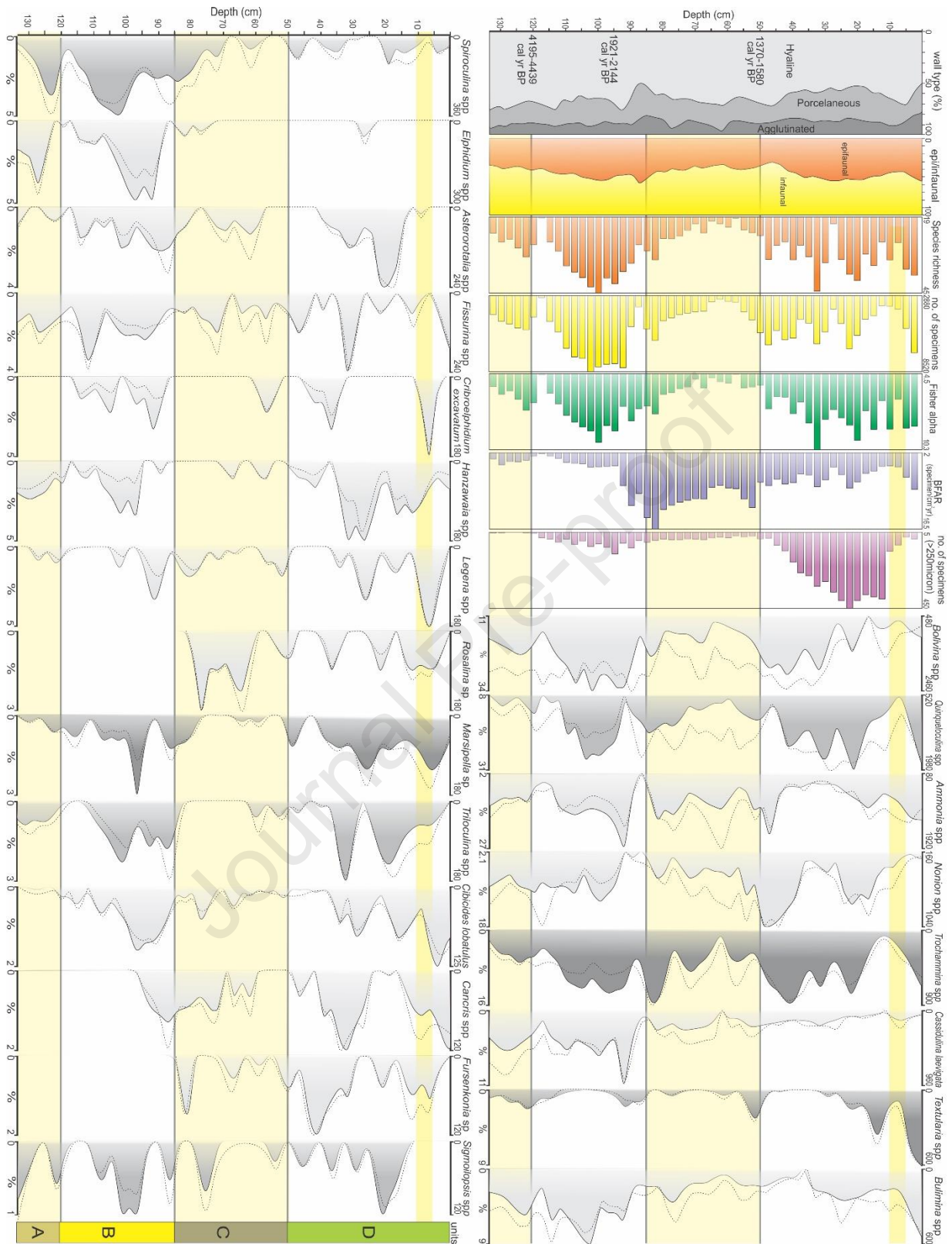
347 that of sand content (42%). The mentioned increases correlate well with the decreasing silt
348 and calcium carbonate contents (7 and 3 % respectively) as well as the sedimentation rate from
349 0.72 to 0.34 mm yr⁻¹.

350

351 **3.4. Foraminiferal assemblages**

352 Seventy different foraminiferal species are recognized, of which 35 are Rotaliida, 21 are
353 Miliolida, 6 are Textulariida, 6 are Legenida, 2 are Lituolida and one is Astrorhizida (A1). The
354 variation in the number of specimens and percentages of benthic foraminiferal taxa are
355 illustrated in figure 5. The assemblages are dominated by hyaline taxa (60%), while
356 porcelaneous (25%) and agglutinated (15%) are placed in the second and third order. Ten most
357 abundant genera are *Bolivina* (26%), *Quinqueloculina* (21%), *Ammonia* (13%), *Nonion* (10%),
358 *Trochammina* (9%), *Cassidulina* (4%), *Bulimina* (4%), *Spiroloculina* (2%), *Textularia* (1%),
359 *Asterorotalia* (1%), *Hanzawaia* (1%) and *Fissurina* (1%). Other subsidiary taxa such as
360 *Triloculina*, *Marsipella*, *Elphidium*, *Cancri*, *Criboelphidium*, *Sigmilopsis*, *Cibicides*,
361 *Lagena*, *Challengerella*, *Rosalina*, *Cornuspira*, *Hyalinea*, *Fursenkoina* comprises <1 - 0.1%
362 of the foraminiferal assemblage. This assemblage is relatively invariant in all of the units. The
363 foraminiferal fauna shows a shelf edge to upper slope association characteristics (Saidova
364 2010, Murray, 2006).

365 As a general trend, the species richness, number of specimens and fisher alpha index
366 (Fisher et al. 1943) of units B and D are much higher than those in units A and C. Mean species
367 richness and number of individuals in the core are 30 and 5200 respectively. Mean species
368 richness in units A and C are 7 - 17% less and in B and C units are 10-17% more than that of
369 the whole core. Unit B represents the highest number of individuals (6670) and units D (5150),
370 A (4850) and C (4150) lie at the next orders. Fisher Alpha index also follows the above
371 arrangement. The frequency of nearly all taxa also follows the above trend. Large specimens
372 (>250 µm) mostly include *A. beccarii* (45%), *Challengerella bradyi* (25%) and *Asterorotalia*
373 *milletti* (20%). *Triloculina tricarinata* and *Spiroloculina depressa* comprise a minor fraction.
374 The number of these specimens is by far highest in unit D (74 - 450; mean: 264), and unit B
375 (53 - 165; mean: 104) lies in second place. The average of this value in two other units is less
376 than 100. The relative average of epifaunal to infaunal taxa in the whole core is 0.82 and shows
377 an increase in units B (0.79) and D (0.96) compared with units A (0.68) and C (0.74).



378

379

380

381

382

Fig. 4. Down-core variations in number (solid areas), and percentage (dashed lines) of foraminiferal taxa. Graphs range between minimum and maximum values along the core sediment. Very light, light and dark grey graphs represent hyaline, porcelaneous and agglutinated taxa respectively.

383 Down-core variation in the frequency of the foraminifera indicates that most of them
 384 are enriched in units B and D. However, these variations in some genera such as
 385 *Quinqueloculina*, *Marsipella*, *Triloculina* and *Cibicides* show a higher magnitude while in
 386 some others (*Bolivina*, *Ammonia*, *Nonion*, *Trochammina*, *Bulimina* and *Fissurina*) have lower
 387 intensity. *Cassidulina*, *Spiroloculina* and *Elphidium* decrease upward, while *Textularia* and
 388 *Fursenkoina* represent a reverse trend. Altogether, the enrichment of individuals in both units
 389 B and D correlates well with the decreasing sedimentation rate. As is demonstrated in Figure
 390 4, BFAR in units D, and especially B, is lower than that of unit C. Indeed, in these units (unlike
 391 unit C) the specimens are relatively less diluted by sedimentation. Therefore, to eliminate the
 392 effect of dilution by sediment deposition, the BFAR and accumulation rate for all foraminiferal
 393 genera were calculated. To compare the BFAR in two distinct sedimentary environments
 394 including 1) units A and C with relatively low MS, sand content, relict particle, SR and high
 395 silt and calcium carbonate content and 2) units B and D with a completely opposing trend, we
 396 calculated the accumulation rate percentage for all foraminifera in units B and D (%AR_{BD})
 397 (Table 3).

$$398 \quad \%AR_{BD} = [(AR_B + AR_D) / (AR_A + AR_B + AR_C + AR_D)] \times 100$$

399 Where %AR_{BD} is the percentage of accumulation rate for specific foraminifera in units
 400 B and D, and AR_A, AR_B, AR_C and AR_D are accumulation rate for the same foraminifera in units
 401 A, B, C and D respectively.

402 Table 3 indicate that the highest %AR_{BD} (>50) mostly belongs to the clinging epifaunal
 403 foraminifera attached above the ambient hard substrate or coarse sediment surface in a high-
 404 energy environment (*Hanzawaia*, *Cibicides Marsipella*, *Hyalinea*, *Textularia*) (Murray 2006,
 405 Schönfeld 2002a). By moving toward the lower values (50 – 43%) free epifaunal taxa living
 406 on a finer substrate (*Asterorotalia*, *Quinqueloculina*, *Trichammina*, *Cornuspira* and *Cancris*)
 407 prevail. The benthic foraminifera with the lowest %AR_{BD} values is dominated by infaunal free
 408 foraminifera living in muddy sediments. These taxa involve *Bolivina*, *Ammonia*, *Nonion*,
 409 *Cassidulina*, *Oolina* and *Fissurina*.

410

411 **Table 3.** Accumulation rate of benthic foraminifera in four units of the core T2S3 and their ecological
 412 characteristics (Murray 2006). The genera are arranged based on %AR_{BD} values

Genera	Mean AR				%AR _{BD}	Mode of life*	Substrate
	Unit A	Unit B	Unit C	Unit D			
<i>Hanzawaia</i>	0.40	0.29	0.27	1.09	67.0	E, C	H

<i>Challengerella</i>	0.00	0.00	0.10	0.20	66.9	E, F	,H
<i>Cibicides</i>	0.00	0.31	0.41	0.50	66.0	E, C	H, HE
<i>Marsipella</i>	0.09	0.27	0.51	0.86	65.5	E, C	H, HE
<i>Criboelphidium</i>	0.00	0.24	0.39	0.40	62.0	I, F	fS/cS
<i>Hyalinea</i>	0.00	0.03	0.20	0.27	60.2	E, F	cS
<i>Triloculina</i>	0.26	0.33	0.62	0.78	55.6	E, F/C	cS
<i>Spirophthalmidium</i>	0.14	0.17	0.00	0.00	55.6	E, F/C	cS
<i>Textularia</i>	0.36	0.14	0.91	1.43	55.3	E, F/C	cS
<i>Fursenkoina</i>	0.00	0.00	0.40	0.50	55.1	I, F	fS
<i>Bulimina</i>	1.59	2.17	3.61	2.47	47.2	I, F	fS/cS
<i>Sigmoilopsis</i>	0.22	0.22	0.44	0.33	46.0	E, F/C	cS
<i>Asterorotalia</i>	0.13	0.39	1.35	0.82	45.0	E, F	cS
<i>quinqueloculina</i>	3.59	6.49	24.12	16.05	44.9	E, F/C	fS/cS
<i>Trochammina</i>	1.70	3.15	10.82	6.49	43.5	E/I, F	fS/cS
<i>Cornuspira</i>	0.10	0.01	0.12	0.16	43.0	E, F	fS/cS
<i>Lagena</i>	0.09	0.11	0.79	0.55	43.0	I, F	fS/cS
<i>Elphidium</i>	0.70	0.81	0.47	0.06	42.7	E/I, F	fS/cS
<i>Cancris</i>	0.00	0.05	0.98	0.67	42.5	E, F	fS/cS
<i>Nonion</i>	3.02	3.25	10.68	6.77	42.2	I, F	fS
<i>Bolivina</i>	7.74	10.56	28.91	15.70	41.7	I, F	fS
<i>Fissurina</i>	0.50	0.63	1.43	0.74	41.3	I, F	fS
<i>Ammonia</i>	3.48	4.56	16.56	7.32	37.2	I, F	fS/cS
<i>Spiroloculina</i>	0.86	1.16	2.14	0.57	36.6	E, F/C	fS/cS
<i>Cassidulina</i>	2.52	2.49	4.57	1.28	34.7	I, F	fS
<i>Oolina</i>	0.00	0.04	0.22	0.00	14.7	I, F	fS

E: epifaunal; I: infaunal; C: clinging; F: free; H: hard substrate; HE: high-energy conditions; fS: fine sediments; cS: coarse sediments; AR: accumulation rate (no. of specimens/cm² 10 yr⁻¹); AR_{BD} : (AR in unit B + AR in unit D) / (AR in whole core) × 100.

413

414 4. Discussion

415 In this section, the variation of the PGDW strength is reconstructed using faunal and non-
 416 faunal proxies, and then, its possible link with the paleoenvironment of SW Asia is evaluated.

417

418 4.1. Application of faunal and non-faunal indicators to reconstruct PGDW variations

419 4.1.1. Non-faunal indicators

420 The PG shows a striking and unique sedimentation pattern which can be employed to correlate
 421 with the hydrodynamic conditions that control sediment transport. The Iranian part is the region
 422 of extensive terrigenous sediment input from occasional violent flash floods building up a
 423 complex coastal plain and covering the northern half of the PG by silt-sized sediments (Baltzer
 424 and Purser 1990; Purser and Seibold 1973). The Arabian shallow shelf, on the contrary, is the
 425 site of intensive and rapid deposition of carbonate sediments which are traceable in bottom

426 sediments of the PG, commonly as sand and pebble fractions (Evans, 1973). These two
427 contrasting sedimentary basins with their specific ecological characteristics come together in
428 the narrow channel of SH. Besides, these modern sediments are mixed with a significant
429 amount of relict sediments, left on the shelf when it was exposed during the last glaciation
430 (Purser and Seibold 1973). Sediment texture and composition becomes more complicated when
431 the influence of density-driven PGDW is considered (Reynolds 1993).

432 Using grain-size and pteropod distribution in 12 sediment cores retrieved from the
433 northern half of the PG, Diester-Haass (1973) suggested that the most reliable indicator of the
434 Holocene climate change are terrigenous materials carried into the PG by rivers. During
435 increased terrigenous supply, the silt-size layer was dominated, while the lesser supply of
436 terrigenous material resulted in the deposition of a coarse-grained layer. Furthermore, the
437 coastal area of mainland and the Qeshm Island is mainly composed of easily erodible Eocene
438 to Miocene limestone rocks such as calcareous sandstone and marls (Molinaro et al. 2004)
439 providing detrital carbonates as a significant fraction of terrigenous sediments (Hamzeh and
440 Farahi Ghasr-Aboonahr 2020; Baltzer and Purser 1990). Volcano-sedimentary units comprise
441 a negligible amount of terrigenous sediments. Hence, unit C in which a co-increase in the
442 amount of silt and carbonate (which is correlated with the SR) takes place corresponds to a
443 relatively humid period with high terrigenous input. Some parts of the PG receiving little recent
444 sedimentation or experiencing high energy bottom currents are characterized by bottom
445 samples containing considerable quantities of skeletal and non-skeletal relict sediments
446 (Diester-Haass 1973). The relict grains, observed in deeper parts of the PG, have a shallow
447 water origin with radiocarbon ages of 7000-13000 years (Sarnthein 1972). A decreasing
448 percentage of sand fraction and relict particles which reflects the degree of dilution by
449 terrigenous materials, together with the decline in the MS values, also confirms the above
450 statement. This situation is observed in unit A with a lesser magnitude as well. Safarkhani et
451 al. (2021) also suggested that these relatively humid periods are well correlated with declining
452 SST at the PG. All the above parameters oscillate conversely in both other units (B and D)
453 indicating a quite different environmental condition. These dry units are contemporaneous to
454 the periods of SST elevation at the PG. During the periods corresponding to units B and D,
455 increasing 1-2°C in SST means increasing heat flux and freshwater loss in the PG, which are
456 the main drivers of the dense water formation and its propagation to the SH. Strengthening the
457 PGDW leads to removing fine sediments and remaining coarser ones as well as the reduction
458 in SR in the mentioned units. However, as the coring site is located at the border, instead of the
459 bottom of the main outflowing channel, the PGDW traces on sediments are modified.

460

461 **4.1.2. Faunal indicators**

462 There have been few studies about the ecology of foraminifera in the PG (Murray 1965, 1966,
463 1970; Basson and Murray 1995; Parker and Gischler 2015), especially at the Iranian sector
464 (Haake 1970, 1975; Nabavi et al. 2014); these studies are patchy and none of them concerned
465 the SH. Some more comprehensive studies (i.e., Amao et al. 2018; Saidova 2010; Cherif et al.
466 1997) have dealt with the nearly entire PG. However, two of the latter covered the SH. The
467 assessed foraminiferal fauna belongs to the continental shelf which is also influenced by the
468 upper slope association. These taxa are very similar to assemblages previously described from
469 the SH and adjacent areas with relatively deeper, warmer, and more oxygenated conditions
470 comparing to other parts of the PG (Amao et al. 2018; Saidova 2010).

471 The observation that a specific assemblage of benthic foraminifera occurs in areas with
472 elevated current velocities (Schönfeld, 2002a, 2002b, 1997) has led to the tentative
473 development of a proxy for bottom current velocity. Investigating down-core variation of
474 benthic foraminifera as the precise indicators of the bottom current strength can provide us
475 with valuable information about bottom paleo-current variations. Coarse grains flooring high-
476 energy areas provide a substrate for attachment of some groups of foraminifera (Kucera 2007;
477 Murray 2006). In these bottom environments, epifaunal foraminifera are relatively abundant
478 and live preferentially on elevated substrates such as coarse shell debris, sponges, crinoids,
479 hydroids, tube worms, or living arborescent benthic foraminifera (e.g., *Rhabdammina* spp.), as
480 well as large terrigenous particles (Kucera 2007; Sen Gupta et al. 2006). These specialized
481 epibenthic foraminifers can also catch suspended organic matter particles (Murray 2006).

482 The number of benthic foraminifera in units A and C is, by far, smaller than that of
483 units B and D. However, this bareness (particularly in unit C) is due to the dilution by high
484 sedimentation rate of terrigenous material. Low BFAR in units B and D may be due to
485 prevailing unfavourable conditions in the corresponding periods. As studies show, high energy
486 bottom currents provide hostile environments, making the number of individuals and species
487 diversity low to moderate (Murray 2006). The increasing proportion of epifaunal foraminifera
488 which is mostly suspension feeder (such as *Hanzawaia*, *Cibicides*, *Marsipella*, *Hyalinea*,
489 *Triloculina* and *textularia*) in Units B and D may be attributed to the domination of high-
490 velocity currents in the corresponding periods. Schönfeld (2002a, 1997) also suggests these
491 assemblages having a high proportion of attached forms are indicative of high-energy shelf
492 areas. The results showed assemblage of sessile epifaunal and/or epibenthic suspension feeders

493 on the Spanish continental margin, influenced by high energy bottom currents related to the
494 Mediterranean Outflow Water. He also indicated a linear correlation between the percentage
495 of typical taxa for elevated microhabitats and bottom water current velocity and used this
496 relation to reconstruct the Holocene history of bottom current velocity at the southern
497 Portuguese margin (Gulf of Cadiz). *Quinqueloculina*, *Asterorotalia*, *Canceris* and
498 *Criboelphidium excavatum* which are commonly observed in sandy substrates (moderate
499 energy) (Murray 2006) are also present as subsidiary taxa in these two high energy units.
500 Saidova (2010) indicated that these taxa (particularly *Quinqueloculina*, *Asterorotalia*, and
501 *Textularia*) show a preference for areas with minimal river discharge in the PG. These units
502 (particularly unit D) also bear the highest percentage of robust tests (>250 μm) (Schönfeld,
503 1997). It is a matter of observation that tests in high-energy environments are thicker-walled
504 and more robust so that they can control their buoyancy. These taxa are highly dependent on
505 the dissolved oxygen and remain of microalgae (phytodetritus) brought by PGDW (Saleh et al.
506 in press). Such a food source of high quality has been observed at 4000 m depth in the Arabian
507 Sea (Pfannkuche et al. 2000). Amao et al. (2018) concluded that the abundance of most of the
508 mentioned epifaunal taxa particularly *Asterorotalia dentata* and some *Elphidium* are positively
509 correlated with nutrient flux. On the other hand, the assemblages resembling Low-energy
510 muddy substrates including *Bolivina*, *Bulimina*, *Nonion*, *Ammonia* and *Cassidulina* (Murray
511 2006) are more abundant taxa in units A and C.

512

513 **4.2. Paleoceanography and paleoclimate of the SH**

514 The bottom sedimentation regime and the magnitude of density difference between the
515 PGDW and the water in the Gulf of Oman (which is the primary driver of water exchange
516 through the SH) are the main oceanographic phenomena of the SH being strongly under the
517 influence of surface temperature of land and sea (which lead to surface evaporation and then
518 dense water formation in the PG). Although IOSW temperature has a considerable role in SST
519 variations in the PG, however, the characteristics of the water masses formed in this landlocked
520 water body are mainly controlled by continental climate (Ghasemifar et al. 2020; Diester-Haass
521 1973). Consequently, the continental climate and IOSW temperatures are the main forcing
522 factor for water circulation (PGDW) and terrigenous sediment input in the SH.

523 Three main parameters of the Earth's orbit around the Sun controlling the seasonal
524 distribution of solar radiation at the top of the atmosphere are: 1) the eccentricity of the orbit
525 with the Sun in one of the two foci, 2) the time of the Earth's passage through its perihelion,

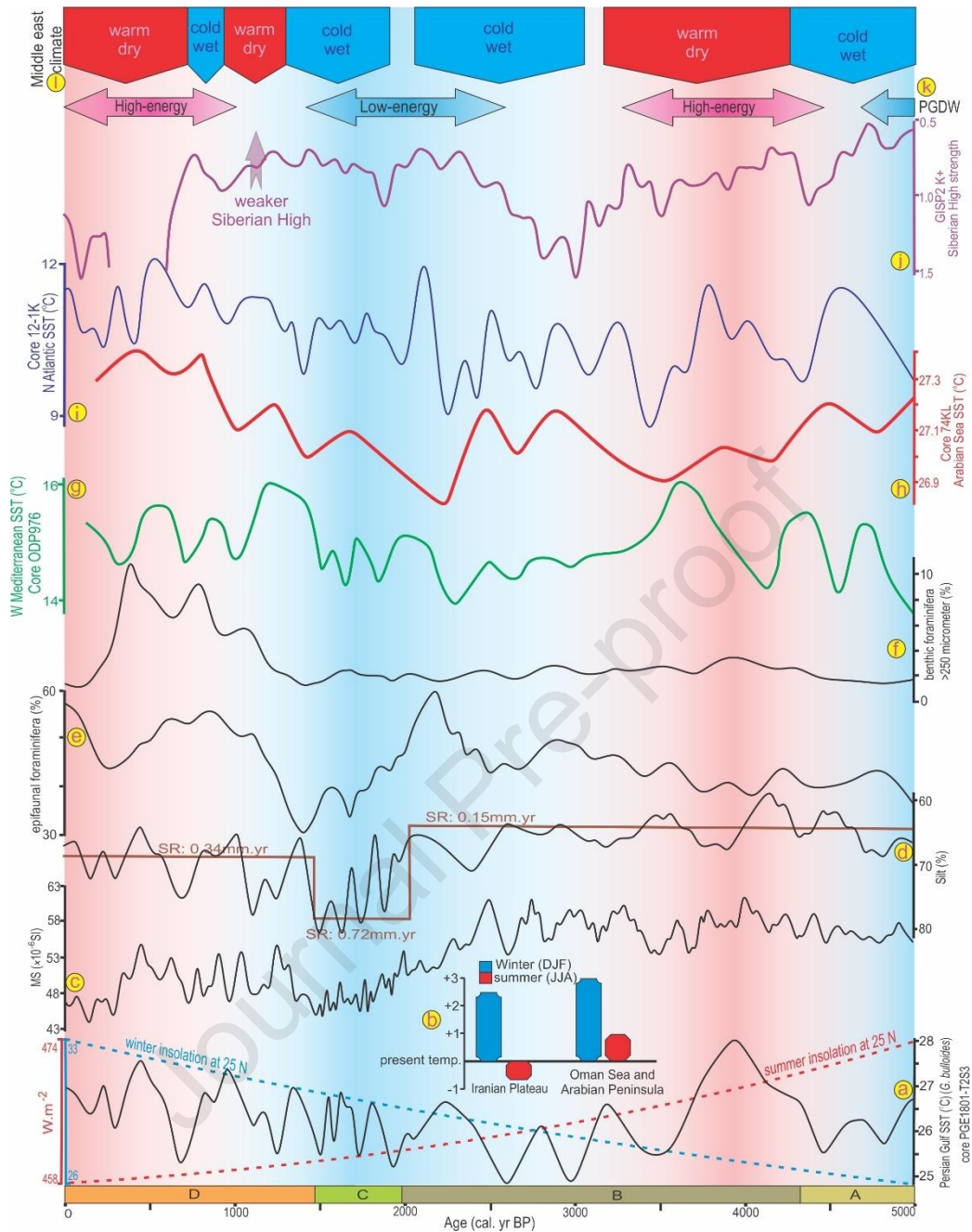
526 and 3) the tilt of its rotation axis (Milankovitch 1941). Over the last 5000 years, precession and
527 obliquity cycles caused a shift of perihelion from late summer to early winter and a decrease
528 in the tilt of the Earth's axis. The resulted radiative changes in the PG area caused a decrease
529 in the boreal summer insolation and an increase in the boreal winter insolation (decreasing
530 seasonality) (Fig. 6a). The seasonally averaged model results of Lorenz et al. (2006) imply that
531 winter warming slightly exceeded the summer cooling in the area, resulting in moderate
532 warming. Present-day warmer tropics (below 30° N) and colder extratropics (above 30° N) on
533 the northern hemisphere compared to the middle Holocene climate is shown by many studies
534 accordingly (Liu et al. 2003; Kim et al. 2004; Lorenz et al. 2006). The PG and the Oman Sea
535 and their surrounding continents are in transitional zones of tropics and extratropics posing
536 complex climate change trends in the area. In the boreal summer, the Arabian Peninsula and
537 the Oman Sea experienced slight warming ($<1^{\circ}\text{C}$), which is in line with the reduction of
538 insolation by 15 W m^{-2} . Simultaneously, there is no Holocene temperature change or moderate
539 cooling over the Iranian Plateau ($<0.7^{\circ}\text{C}$) (Figure 6b). In the boreal winter, the Iranian Plateau,
540 the Arabian Peninsula and the PG and the Oman Sea generally exhibit pronounced warming of
541 $2.5 - 3^{\circ}\text{C}$. this gradual warming especially in winter (the season of PGDW formation in
542 northwest and south of the PG) may be responsible for a general trend of increasing PGDW
543 intensity since the mid-Holocene. Kim et al. (2004) also suggest that the Holocene weakening
544 of the Arctic Oscillation/North Atlantic Oscillation (AO/NAO) pattern is associated with the
545 tropical warming caused by the precession-related increasing boreal winter insolation. In boreal
546 winter, a considerable mid-Holocene decrease evolved in sea level pressure difference between
547 high latitudes (Icelandic low) and low latitudes including the continents bordering the PG
548 (Azores high) (Lorenz et al. 2006). The climate models linked this decrease in east-west surface
549 temperature difference with a Holocene weakening of the midlatitude atmospheric circulation,
550 and therefore, reducing westerlies into the area. Altogether, the overall outcome of orbitally-
551 driven solar insolation changes has been a gradual warming and weakening inflow of cold
552 continental air masses primarily in winter (Felis et al. 2000) over the area since the last 5
553 millennia (Fig. 6a). However, as Mayewski et al. (2004) indicate, some short-term centennial-
554 scale rapid climate change events disrupt this general warming trend. They suggest that solar
555 variability superimposed on long-term changes in insolation seems to be the most likely
556 responsible for these changes. The most notable instance is an abrupt SST increase centred at
557 3.8 cal kyr BP. A decline in ^{10}Be concentrations in the GISP2 ice core attributes this event to
558 increasing solar output. This sudden SST elevation is traceable in the North Atlantic and
559 western Mediterranean Sea (Fig. 6f and h).

560 Periods of high SST in the PG coincide with the increasing continental temperature and
561 dryness over SW Asia and, in turn, a decline in terrigenous input to the PG and SH. The recent
562 paleoclimate studies show, unlike the climate conditions during the early Holocene, ISM
563 intensification during mid to late Holocene have harmed the hydroclimate regime of S Iran
564 (Miller et al. 2016; Hamzeh and Farahi Ghasr-Aboonasar 2020). During the warm episodes,
565 northward migration of the ITCZ and an intensification of the ISM system results in earlier
566 spring maximum precipitation and a later autumn maximum precipitation (extending the length
567 of the summer dry season), and therefore, increased drought (Djamali et al. 2010). In
568 conclusion, paleotemperature changes in SW Asia (both continental and oceanic) can directly
569 influence the variation of terrigenous input and PGDW of the SH.

570

571 **4.2.1. Unit A: ~5000 – 4300 cal yr BP**

572 Due to the lack of radiocarbon dating, the basement age of the core T2S3 is rather unclear.
573 Indeed, its corresponding ~700-year period is the end of an SST decreasing trend started from
574 the early-Holocene, and the beginning of an SST increase documented in the SH (Safarkhani
575 et al. 2021), the Arabian Sea (Saher et al. 2007) and the North Atlantic Ocean (Kim et al. 2004)
576 due to the reduction of summer solar insolation (Mayewski et al. 1997). During this period
577 when the mean annual SST in the SH was 26.2°C (~1°C lower than that of today), the Arabian
578 Sea salinity also decreased (Dooze-Rolinski et al. 2001). A slight increase in terrigenous input
579 is observed in this area which is contemporaneous to the optimum climate of the Iranian plateau
580 and Near East (Bar-Matthews et al. 2003; Frumkin et al. 1991). Vaezi et al. (2018) showed a
581 decrease in aeolian input together with an abrupt increase in rainfall between 5 and 4.7 cal kyr
582 BP in the Hamun-e Jazmurian basin, about 140 km northeast of the SH. This optimal climate
583 caused the flourishing of Bronze Age civilizations from Mesopotamia toward SE Iran and is
584 attributed to the ISM-induced precipitations (Fleitmann et al. 2007; Cullen et al. 2000). As the
585 proxies such as moderate increasing upward MS value, sand content and epifaunal
586 communities as well as moderate decreasing upward in silt content show, a decline in SST of
587 the PG and, in turn, eliminating SST contrast between PG and the Arabian Sea and reduction
588 of evaporation rate caused PGDW strength to become moderate to low. Considering that this
589 unit occurred just 2-3 thousand years after postglacial sea-level rise inundation, BFAR has been
590 lower than that of subsequent units. Altogether, this period was wetter and colder than that of
591 today and lower SST of the SH (due to colder continental climate and IOSW) led to decrease
592 PGDW intensity (Fig. 7).



593

594 **Fig. 6.** Comparison of (a) Mg/Ca-derived SST in the SH measured in tests of *G. bulloides* from PGE1801-T2S3
 595 sediment core (Safarkhani et al. 2021) as well as summer and winter insolation at 25°N (Berger and Loutre 1991),
 596 (c) MS values with (d) silt content and sedimentation rate, (e) per cent of epifaunal foraminifera, and (f) per cent
 597 of >250 μm benthic foraminifera of the SH from PGE1801-T2S3 sediment core (this study). Furthermore,
 598 paleoclimate records from the surrounding regions, including (g) SST record from the western Mediterranean Sea
 599 (Català et al. 2019), (h) SST record from the Arabian Sea (Sirocko et al. 1993), (i) SST record from the North
 600 Atlantic (Kim et al. 2004), (j) Siberian High intensity (Mayewski et al. 2004), (k) the estimated PGDW condition
 601 (l) and climate record of the Middle East (Issar, 2004) are represented. b): Comparison of summer and winter
 602 surface temperature change (in °C) in 30° N (Iranian Plateau) and 25° N (Arabian Peninsula and the Oman Sea)
 603 since the mid-Holocene.

604

605 4.2.2. Unit B: 4300 – 2000 cal yr BP

606 This period begins with an abrupt increase in SST of the SH, as well as the
607 Mediterranean Sea (Català et al. 2019) likely due to solar irradiance (Mayewski et al. 2004).
608 Nonetheless, the mean annual SST of the Arabian Sea is lower than both above mentioned.
609 This significant warming is also documented in the Near East by a prolonged drought (Issar
610 2004). The high aeolian input, high salinity, and rise in evaporite minerals were detected around
611 4.3 cal kyr BP in lake sediments of Hamun-e Jazmurian suggesting a dry condition (Vaezi et
612 al. 2018). At the same time, Bronze Age civilization in the southeast and east of Iran evanesced.
613 Using palynology of a peat bog close to Konar Sandal archaeological site (150 km north of
614 SH), Gurjazkaite et al. (2018) detected a drought period ended at 3.8 cal kyr BP. Cullen et al.
615 (2000) indicated that climate deterioration in the Middle East around 4.2 cal kyr BP led to the
616 demise of the Akkadian Empire. Paleoceanography of the Red Sea indicates that terrigenous
617 input and SR in this period was lower than the periods before and after that. The destructive
618 effects of weakened ISM (expansion of summer season) may be considered as responsible for
619 climate deterioration in this warm period (Miller et al. 2016; Djamali et al. 2010).

620 Varying faunal and non-faunal indicators such as increasing MS value, sand content
621 and epifaunal communities as well as decreasing silt content demonstrate a gradual increase in
622 PGDW strength which may be attributed to an abrupt SST increase in the SH and its relatively
623 high discrepancy with the Arabian Sea (Fig. 6 and g). Since 3.5 cal kyr BP, SST started to
624 decline gradually which was accompanied by an increasing terrigenous input. Paleoclimate
625 researches suggest that southward migration of ITCZ has caused the higher ISM-induced
626 precipitations were replaced by lower MLW-induced Mediterranean winter precipitations
627 (Fleitmann et al. 2007; Hamzeh et al. 2006). The decreasing trend of the PG SST in this period
628 is in agreement with the gradual decrease in SST of the Red Sea and the Mediterranean Sea,
629 and also a decrease in the strength of the Siberian High (Mayewski et al. 1997). This wetter
630 condition is consistent with an increase in the water level of the Dead Sea and the Lake Van
631 (Wick et al., 2003; Frumkin et al. 1991), and enhancing Tigris and Euphrates discharge (Kay
632 and Johnson, 1981). In general, as the mean SST of this period is lower than that of Unit D
633 (the last 1450 years), and Arabian Sea SST slightly decreases (Fig. 6g) causing a decline in
634 SST contrast between the PG and the Arabian Sea, the variation magnitude of PGDW proxies
635 is relatively low. Relatively lower winter isolation (reduction of saline water originated from
636 northwest of the PG and the Arabian shallow shelf) compared to present time provides another
637 hint that PGDW intensity during this period was lower than that of today. Altogether, at this

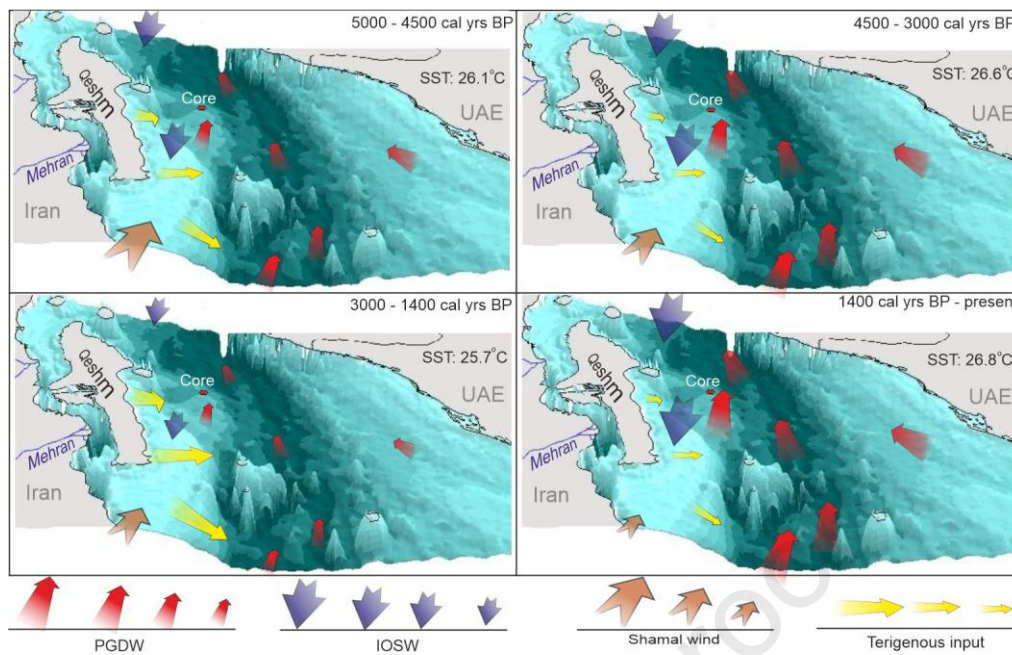
638 time, the PGDW is rather weaker and terrigenous input is higher than that of the corresponding
639 period of unit D.

640

641 **4.2.3. Unit C: 2000 – 1450 cal yr BP**

642 SST cooling, PGDW weakening and terrigenous input (and also SR) increasing trend, started
643 about 1500 years earlier, reach their highest values in this period. Paleoclimate reconstruction
644 indicates that SST from 3.5 to 1.5 cal kyr BP is about 2°C lower than that of today (Safarkhani
645 et al. 2021). This SST variation trend is also traceable in the Arabian Sea, the Mediterranean
646 Sea and the North Atlantic (Fig. 6g, h and i). Paleoclimate study in Khuran Estuary (north of
647 Qeshm Island) demonstrates that during this time the discharge of the rivers inflowing to the
648 Strait of Hormoz has been much higher than today (Hamzeh and Farahi Ghasr-Aboonahr,
649 2020). Miller et al. (2016) suggested a high amount of freshwater discharge and low dust input
650 into the Oman Sea during this time. Arz et al. (2003) also indicated that during this time interval
651 the river discharge in the Red Sea basin reached the maximum over the last 5000 years. During
652 the same period, a climate optimum documented in various archives e.g., sediments of caves,
653 lakes, and seas in the Middle East period (Bar-Matthews et al. 2003; Wick et al. 2003; Frumkin
654 et al. 1991). It seems that, because summer insolation decreased and winter insolation was still
655 lower than that of today (Fig. 6a) the evaporation rate (as the forcing factor of penetrating the
656 IOSW (Reynolds, 1993)) decreased, and therefore, the overall PGDW intensity was relatively
657 low (Fig. 7). This time of high river inflow and low-energy PGDW provided a favourable
658 condition for the expansion of benthic foraminifera (mostly infaunal taxa such as *Bolivina*,
659 *Ammonia*, *Bulimina* and *Lagena*).

660



661

662 **Fig. 7.** 3D map of the SH showing the intensity of inflowing surface currents, bottom currents, Shamal wind and
 663 the amount of terrigenous input over the last 5000 years.

664

665 4.2.4. Unit D: 1450 cal yr BP to present

The highest average SST of the PG is recorded over the last 1450 year (mean: 26.7°C), which is consistent with the general trend of increased SST in the neighbouring water bodies, such as the Arabian Sea, the Red Sea, and the Mediterranean Sea, which are all marked by notable fluctuations. This period is synchronous with a gradual and oscillating deterioration of the climate all over the Middle East (Issar 2004). Based on the isotopic composition of the stalagmites in Soreq Cave, Bar-Matthews et al. (2003) showed that the average annual precipitation over the eastern Mediterranean began to decrease sometime after 1400 cal yr BP. A relatively high SST in the area is the forcing factor for reinforcement of PGDW which has the strongest bottom currents during the last 5000 years. This is reinforced by the highest winter isolation in the Holocene, which possibly increases the outflow of saline water from the northwestern and southern shallow shelves, and by a decline in the intensity of Shamal winds (Felis et al. 2000) during winter which may increase the IOSW inflow. Although high energy bottom currents provide a harsh environment for benthic fauna, they bring oxygenated water together with phytodetritus particles for the persistence of foraminifera (mostly large epifaunal suspension feeders). After unit C, this unit comprises the most BFAR of the last 5000 years.

SST warming trend is disrupted by a prominent SST cooling (~700-600 cal yr BP) which can be traced back, with a multi-decade age difference, to the Mediterranean Sea. This period which led to an increase in the input of terrigenous sediments into the PG, taking the age uncertainties into account, appears to be related to the Little Ice Age (LIA) cold spell in the Northern Hemisphere. Such a condition has been also reported by Leroy et al. (2011) in Anzali and Amirkola lagoons (southern coasts of the Caspian Sea). A palynological investigation conducted by Miller et al. (2016) indicated a shift from desert to grassland vegetation, implying wetter conditions during the LIA in southern Iran. This short period is also recognizable by the reduction of the number of foraminifera, particularly epifaunal taxa. It may be attributed to a short time reduction in PGDW strength and higher terrigenous input.

666 5. Conclusions

The present paper, for the first time, reconstructs paleocurrent strength variations of PGDW in the SH and its connection with the paleoclimate of SW Asia. Since the mid-Holocene, precession-related increasing boreal winter insolation caused a long-term SST increase, while solar variability was responsible for short-term SST changes. During the periods of reduced SST, the bottom current energy of PGDW decreases and a notable increase occurs in river discharges into the area. Finer sediment deposition in a relatively low energy bottom provides a favourable environment for benthic foraminifera (dominated by infaunal taxa). Conversely, during the episodes of increased SST in the SH and warming in the surrounding lands which are associated with climate aridity in the Middle East and the Iranian Plateau, PGDW strength increases. The general SST warming in the PG is concordant with the winter insolation increase, and in turn, the decline in the inflow of cold air masses to the area. The periods of high winter isolation cause increasing outflow of saline water from the northwestern and southern shallow shelves and reducing the intensity of Shamal winds (Felis et al. 2000) which elevates the IOSW inflow. High energy bottom currents in these periods cause the domination of epifaunal foraminifera. However, these high DO and phytodetritus content bottom currents cause propagation of robust suspension feeder epifaunal taxa. Indeed, as Hamzeh and Farahi Ghasr-Aboonasr (2020) and Miller et al. (2016) concluded, the progressive global warming trend causing climate aridity (due to extending summer length) is linked to the increasing SST and PGDW intensification in the PG and SH basin.

667

668 Acknowledgements

669 This study is an integral part of a comprehensive study of the Persian Gulf Explorer research
670 project, supported by the Iranian National Institute for Oceanography and Atmospheric
671 Science, with financial support from Lorestan University. The authors would like to thank the
672 crew staff of R/V Persian Gulf Explorer, especially Mr S. Sanjani and Dr A. Saleh as technical
673 and scientific managers respectively.

674

675 References

- 676 Al-Ghadban, A.N., Abdali, F. and Massoud, M.S. (1998). Sedimentation rate and bioturbation
677 in the Arabian Gulf. *Environment International* 24(1-2): 23-31.
- 678 Al-Said, T., Yamamoto, T., Madhusoodhanan, R., Al-Yamani, F. and Pokavanich, T. (2018).
679 Summer hydrographic characteristics in the northern ROPME Sea Area: Role of ocean
680 circulation and water masses. *Estuarine, Coastal and Shelf Science* 213: 18-27.
- 681 Amao, A.O., Kaminski, M.A., Rostami, M.A., Mahmudi-Gharaie, M.H., Lak, R. and
682 Frontalini, F. (2019). Distribution of benthic foraminifera along the Iranian coast. *Marine*
683 *Biodiversity* 49(2): 933-946.
- 684 Arz, H.W., Lamy, F., Patzold, J., Muller, P.J. and Prins, M. (2003). Mediterranean Moisture
685 Source for an Early-Holocene Humid Period in the Northern Red Sea. *Science* 300: 118-
686 121.
- 687 Azizpour, J., Chegini, V., Khosravi, M. and Einali, A. (2014). Study of the physical
688 oceanographic properties of the Persian Gulf, Strait of Hormuz and Gulf of Oman based
689 on PG-GOOS CTD measurements. *Journal of the Persian Gulf* 5(18): 37-48.
- 690 Baltzer, F. and Purser, B.H. (1990). Modern alluvial fan and deltaic sedimentation in a foreland
691 tectonic setting: the lower Mesopotamian plain and the Arabian Gulf. *Sedimentary*
692 *Geology* 67(3-4): 175-197.
- 693 Bar-Matthews, M., Ayalon, A., Gilmour, M., Matthews, A., Hawkesworth, C.J. (2003).
694 Sealand oxygen isotopic relationships from planktonic foraminifera and speleothems in
695 the Eastern Mediterranean region and their implication for paleorainfall during interglacial
696 intervals. *Geochimica et Cosmochimica Acta* 67: 3181-3199.
- 697 Basson, P.W., and Murray, J. (1995). Temporal variations in four species of intertidal
698 foraminifera, Bahrain, Arabian Gulf. *Micropaleontology* 41: 69-76.

- 699 Berger, A., Loutre, M. F. (1991). Insolation values for the climate of the last 10 million years.
700 *Quaternary Science Reviews* 10: 297-317.
- 701 Blaauw, M., 2010. Methods and code for 'classical' age-modelling of radiocarbon
702 sequences. *Quaternary Geochronology* 5, 512-518.
- 703 Bower, A.S., Hunt, H.D. and Price, J.F. (2000). Character and dynamics of the Red Sea and
704 Persian Gulf outflows. *Journal of Geophysical Research: Oceans* 105(C3): 6387-6414.
- 705 Bruthans, J., Filippi, M., Geršl, M., Zare, M., Melková, J., Pazdur, A., Bosák, P. (2006).
706 Holocene marine terraces on two salt diapirs in the Persian Gulf, Iran: age, depositional
707 history and uplift rates. *Journal of Quaternary Science: Published for the Quaternary*
708 *Research Association* 21: 843–857.
- 709 Català, A. Cacho, I., Frigola, J., Pena, L.D. and Lirer, F. (2019) Holocene hydrography
710 evolution in the Alboran Sea: a multi-record and multi-proxy comparison. *Climate of the*
711 *Past* 15: 927-942.
- 712 Cherif, O.H., Al-Ghadban, A.N., Al-Rifaiy, I.A. (1997) Distribution of foraminifera in the
713 Arabian Gulf. *Micropaleontology* 43: 253–280.
- 714 Cullen, H.M., deMenocal, P.B., Hemming, S., Hemming, G., Brown, F.H., Guilderson, T. and
715 Sirocko, F. (2000) Climate change and the collapse of the Akkadian empire: Evidence
716 from the deep sea. *Geology* 28(4), 379-382.
- 717 Diester-Haass, L. (1973). Holocene climate in the Persian Gulf as deduced from grain size and
718 petropod distribution. *Marine Geology* 14: 207- 223.
- 719 Djamali, M., Akhiani, H., Andrieu-Ponel, V., Braconnot, P., Brewer, S., de Beaulieu, J.-L.,
720 Fleitmann, D., Fleury, J., Gasse, F., Guibal, F., Jackson, S.T., Lézine, A.-M., Médail, F.,
721 Ponel, P., Roberts, N., Stevens, L., 2010. Indian Summer Monsoon variations could have
722 affected the early-Holocene woodland expansion in the Near East. *Holocene* 20, 813-820.
- 723 Dooze-Rolinski, H., Rogalla, U., Scheeder, G., Luckge, A. and von Rad, U. (2001). High-
724 resolution temperature and evaporation changes during the late Holocene in the
725 northeastern Arabian Sea. *Paleoceanography* 16(4): 358-367.
- 726 Evans, G., Murray, J.W., Biggs, H.E.J., Bate, R. and Bush, P.R. (1973). The oceanography,
727 ecology, sedimentology and geomorphology of parts of the Trucial Coast barrier island
728 complex, Persian Gulf. In *The Persian Gulf* (pp. 233-277). Springer, Berlin, Heidelberg.
- 729 Felis, T., Pätzold, J., Loya, Y., Fine, M., Nawar, A.H. and Wefer, G. (2000). A coral oxygen
730 isotope record from the northern Red Sea documenting NAO, ENSO, and North Pacific
731 teleconnections on Middle East climate variability since the year 1750, *Paleoceanography*,
732 15, 679– 694.

- 733 Fisher, R.A., Corbet, A.S., and Williams, C.B. (1943). The relation between the number of
734 species and the number of individuals in a random sample of an animal population. *J.*
735 *Anim. Ecol.* (1): 42–58.
- 736 Fleitmann, D., Burns, S.J., Mangini, A., Mudelsee, M., Kramers, J., Villa, I., Neff, U., Al-
737 Subbary, A.A., Buettner, A., and Hippler, D. (2007). Holocene ITCZ and Indian monsoon
738 dynamics recorded in stalagmites from Oman and Yemen (Socotra). *Quaternary Science*
739 *Reviews* 26: 170-188.
- 740 Frumkin, A., Magaritz, M., Carmi, I. and Zak, I. (1991). The Holocene climatic record of the
741 salt caves of Mount Sedom, Israel. *The Holocene* 1: 191–200.
- 742 Ghasemifar, E., Farajzadeh, M., Mohammadi, C. and Alipoor, E. (2020). Long-term change of
743 surface temperature in water bodies around Iran–Caspian Sea, Gulf of Oman, and Persian
744 Gulf–using 2001–2015 MODIS data. *Physical Geography* 41(1): 21-35.
- 745 Gurjazkaite, K., Routh, J., Djamali, M., Vaezi, A., Poher, Y., Beni, A.N., Tavakoli, V. and
746 Kylin, H. (2018). Vegetation history and human-environment interactions through the late
747 Holocene in Konar Sandal, SE Iran. *Quaternary Science Reviews* 194: 143-155.
- 748 Gupta, A.K., David M. Anderson, D.M. and Overpeck, J.T. (2003). Abrupt changes in the
749 Asian southwest monsoon during the Holocene and their links to the North Atlantic Ocean.
750 *Nature* 421(23): 354-357.
- 751 Haake, F. (1975). Miliolinen (Foram) in oberflachensedimenten des Persischen Golfes.
752 "Meteor" Forsch-Ergebnisse 21: 15–51.
- 753 Haake, F.W. (1970). Zur Tiefenverteilung von Miliolinen (Foram.) im Persischen Golf.
754 *Paläontol Z* 44: 196–200.
- 755 Hahipour, A., Fontugne, M. (1993). Quaternary uplift of Qeshm Island (Iran). *Comptes*
756 *Rendus de l'Académie des Sciences, Paris* 317 (II): 419–424.
- 757 Hamzeh, M.A. in press. Environmental implications of the distribution and physical
758 characteristics of surface sediments in the northern Persian Gulf. *Geo-Marine Letters*.
- 759 Hamzeh, M.A., Gharai, M.H.M., Lahijani, H.A.K., Djamali, M., Harami, R.M. and Beni, A.N.
760 (2016). Holocene hydrological changes in SE Iran, a key region between Indian Summer
761 Monsoon and Mediterranean winter precipitation zones, as revealed from a lacustrine
762 sequence from Lake Hamoun. *Quaternary International* 408: 25-39.
- 763 Hamzeh, M.A. and Farahi Ghasr-Aboonahr, S. (2020). Palaeoenvironmental changes in the
764 Khuran Estuary of SE coastal Iran during the last two millennia, based on the analysis of
765 a sediment core. *Palaeogeography, Palaeoclimatology, Palaeoecology* 542: 109563.

- 766 Haynes, J.R., (1981). Foraminifera. McMillan Publishers LTD, London and Basingstoke,
767 475p.
- 768 Heiri, O., Lotter, A.F. and Lemcke, G. (2001). Loss on ignition as a method for estimating
769 organic and carbonate content in sediments: reproducibility and comparability of results.
770 *Journal of Paleolimnology* 25: 101-110.
- 771 Herguera, J. C. (1992). Deep-sea benthic foraminifera and biogenic opal: Glacial to postglacial
772 productivity changes in the western equatorial Pacific, *Marine Micropaleontology* 18: 79-
773 98.
- 774 Hollister, C. D., & Heezen, B. C. (1972). Geologic effects of ocean bottom currents: Western
775 North Atlantic. In: A. L. Gordon (Ed.), *Studies in physical oceanography* (Vol. 2, pp. 37–
776 66). New York: Gordon and Breach.
- 777 Hunter, J.R. (1986). The physical oceanography of the Arabian Gulf: a review and theoretical
778 interpretation of previous observations. In: *Marine Environment and Pollution*.
779 *Proceedings 1st Arabian Gulf Conference on Environmental Pollution*. Kuwait University,
780 Kuwait, pp. 1-23.
- 781 IWRMC (2016). Report on Water Resources Yields in Bandar Abbas District (code: 2801),
782 Feb. 2016. Report no. 300-28-RPT-WB-Ba-02. Sangab Zagros Consulting Engineers, Iran
783 Water Resource Management Co (70p).
- 784 Issar, A.S. (2004). *Climate Changes during the Holocene and their Impact on Hydrological*
785 *Systems*, Cambridge University Press, Cambridge.
- 786 Johns, W.E., Yao, F. and Olson, D.B. (2003). Observations of seasonal exchange through the
787 Straits of Hormoz and the inferred heat and freshwater budgets of the Persian Gulf. *Journal*
788 *of Geophysical Research* 108(12): 1-18.
- 789 Kessler, P. (1973). The structural and geomorphic evolution of the Persian Gulf. In *The Persian*
790 *Gulf* (pp. 11-32). Springer, Berlin, Heidelberg.
- 791 Kay, P.A. and Johnson, D.L. (1981). Estimation of Tigris-Euphrates streamflow from regional
792 paleoenvironmental proxy data. *Climatic Change* 3: 251-263.
- 793 Khosravi, M., Siadatmousavi, S.M., Vennell, R., Chegini, V. (2018) The transverse dynamics
794 of flow in a tidal channel within a greater strait. *Ocean Dynamics* 10236-017-1127-3
- 795 Kim, J.-H., Rimbu, N., Lorenz, S.J., Lohmann, G., Nam, S.-I., Schoutene, S., Ruhlemann, C.
796 and Schneider, R.R. (2004) North Pacific and North Atlantic sea-surface temperature
797 variability during the Holocene. *Quaternary Science Reviews* 23: 2141-2154.
- 798 Kodera, K. (2004). Solar influence on the Indian Ocean Monsoon through dynamical
799 processes. *Geophysical Research Letters* 31(24): L24209.

- 800 Konert, M., Vandenberghe, J. (1997). Comparison of laser grain size analysis with pipette and
801 sieve analysis: a solution for the underestimation of the clay fraction. *Sedimentology* 44:
802 523-535.
- 803 Kucera, M. (2007). Planktonic foraminifera as tracers of past oceanic environments, In:
804 *Developments in marine geology* 1: 213-262.
- 805 Leroy, S.A.G., Lahijani, H.A.K., Djamali, M., Naqinezhad, A., Moghadam, M.V., Arpe, K.,
806 Shah-Hosseini, M., Hosseindoust, M., Miller, C.S., Tavakoli, V., Habibi, P. and Naderi
807 Beni, M. (2011). Late Little Ice Age palaeoenvironmental records from the Anzali and
808 Amirkola Lagoons (south Caspian Sea): Vegetation and sea level changes.
809 *Palaeogeography, Palaeoclimatology, Palaeoecology* 302: 415-434.
- 810 Liu, Z., Brady, E., and Lynch-Stieglitz, L. (2003). Global ocean response to orbital forcing in
811 the Holocene, *Paleoceanography*, 18(2): 1041, doi:10.1029/2002PA000819.
- 812 Loeblich, A.R., Tappan, H. (1988). *Foraminiferal Genera and Their Classification*. Springer
813 Science Business Media New York (2045p).
- 814 Lorenz, M., Klingbeil, K. and Burchard, H. (2020). Numerical study of the exchange flow of
815 the Persian Gulf using an extended total exchange flow analysis framework. *Journal of*
816 *Geophysical Research: Oceans* 125(2). doi:10.1029/2019JC015527.
- 817 Lorenz, S.J., Kim, J.H., Rimbu, N., Schneider, R.R. and Lohmann, G. (2006). Orbitally driven
818 insolation forcing on Holocene climate trends: Evidence from alkenone data and climate
819 modeling. *Paleoceanography*, 21(1). PA1002, doi:10.1029/2005PA001152.
- 820 Lutze, G. F., and Altenbach, A. (1988). *Rupertina stabilis* (WALLICH), a highly adapted,
821 suspension feeding foraminifer. *Meyniana*, 40: 55–69.
- 822 Majidzadeh, Y. 2003, *Jiroft: The Earliest Oriental Civilization: Printing and Publishing of the*
823 *Ministry of Culture and Islamic Guidance, Tehran* 69–103.
- 824 Mayewski, P.A., Meeker, L.D., Twickler, M.S., Lyons, W.B., and Prentice, M. (1997). Major
825 features and forcing of high-latitude northern hemisphere atmospheric circulation using a
826 110,000-year-long glaciochemical series. *J. Geophys. Res* 102: 26,345 - 26,366.
- 827 Mayewski, P.A., Rohling, E.E., Stager, J.C., Karlén, W., Maasch, K.A., Meeker, L.D.,
828 Meyerson, E.A., Gasse, F., van Kreveld, S. and Holmgren, K. (2004). Holocene climate
829 variability. *Quaternary Research* 62(3)): 243-255.
- 830 McCave, I.N. 2007. Deep-sea sediment deposits and properties controlled by
831 currents. *Developments in Marine Geology* 1: 19-62.
- 832 Milankovitch, M.K. (1941). *Kanon der Erdbestrahlung und seine Anwendung auf das*
833 *Eiszeitenproblem*. Royal Serbian Academy Special Publication 133, pp.1-633.

- 834 Miller, C.S., Leroy, S.A.G., Collins, P.E.F. and Lahijani, H.A.K. (2016). Late Holocene
835 vegetation and ocean variability in the Gulf of Oman. *Quaternary Science Reviews* 143:
836 120-132.
- 837 Molinaro, M., Guezou, J.C., Leturmy, P., Eshraghi, S., de Lamotte, D.F. (2004). The origin of
838 changes in structural style across the Bandar Abbas syntaxis, SE Zagros (Iran). *Mar. Pet.*
839 *Geol.* 21, 735–752.
- 840 Mudroch, A., Azcue, J.M., Mudroch, P. (1997). *Manual of Physico-Chemical Analysis of*
841 *Aquatic Sediments*. Lewis Publishers, CRC Press, USA (287p).
- 842 Murray, J.W. (1965). The foraminifera of the Persian Gulf. Part I. *Rosalina adhaerens* sp.
843 nov. *Annals and Magazine of Natural History*, 8(86): 77-79.
- 844 Murray, J. (1966). The Foraminifera of the Persian Gulf. 5. The shelf off the tracial coast.
845 *Palaeogeogr Palaeoclimatol Palaeoecol* 2: 267–278
- 846 Murray, J. (1970). The Foraminifera of the Persian Gulf: 6. Living forms in the Abu Dhabi
847 region. *J Nat Hist* 4: 55–67
- 848 Murray, J.W., 2006. *Ecology and Applications of Benthic Foraminifera*. Cambridge University
849 Press (426p).
- 850 Nabavi, S.M.B., Moosapanah, S.G.R., Rajab Zadeh Ghatrami, E., Ghayyem Ashrafi, M. and
851 Nabavi, S.N. (2014). Distribution, Diversity and Abundance of Benthic Foraminifera of
852 the Northwestern Persian Gulf. *Journal of the Persian Gulf* 5(16): 15-26.
- 853 Olsen, J., Ascough, P., Loughheed, B.C., Rasmussen, P. (2017). Radiocarbon dating in estuarine
854 environments. In: *Applications of Paleoenvironmental Techniques in Estuarine Studies*.
855 Springer, pp. 141–170.
- 856 Parker, J.H., Gischler, E. (2015). Modern and relict foraminiferal biofacies from a carbonate
857 ramp, offshore Kuwait, northwest Persian Gulf. *Facies* 61: 1-22.
- 858 Pfannkuche, O., Sommer, S. and Kähler, A. (2000). Coupling between phytodetritus deposition
859 and the small-sized benthic biota in the deep Arabian Sea: analyses of biogenic sediment
860 compounds. *Deep Sea Research Part II: Topical Studies in Oceanography* 47(14): 2805-
861 2833.
- 862 Pirazzoli, P.A., Reyss, J.L., Fontugne, M., Haghypour, A., Hilgers, A., Kasper, H.U., Nazari,
863 H., Preusser, F. and Radtke, U. (2004). Quaternary coral-reef terraces from Kish and
864 Qeshm Islands, Persian Gulf: new radiometric ages and tectonic implications. *Quaternary*
865 *International* 120(1): 15-27.

- 866 Potts, D.T., Lamberg-Karlovski, C., Pittman, H., Kohl, P.L. (2001). Excavations at Tepe
867 Yahya, Iran, 1967–1975: the third millennium: Peabody Museum of Archaeology, v. 45,
868 p. 85–146.
- 869 Pous, S., Lazure, P., and Carton, X. (2015). "A model of the general circulation in the Persian
870 Gulf and in the Strait of Hormuz: Intraseasonal to interannual variability." *Continental
871 Shelf Research* 94, 55-70.
- 872 Purser, B.H. and Seibold, E. (1973). The principal environmental factors influencing Holocene
873 sedimentation and diagenesis in the Persian Gulf. In *The Persian Gulf* (pp. 1-9). Springer,
874 Berlin, Heidelberg.
- 875 Regard, V., Bellier, O., Braucher, R., Gasse, F., Bourlès, D., Mercier, J., Thomas, J.C., Abbassi,
876 M.R., Shabanian, E. and Soleymani, S. (2006). ^{10}Be dating of alluvial deposits from
877 Southeastern Iran (the Hormoz Strait area). *Palaeogeography, Palaeoclimatology,
878 Palaeoecology* 242(1-2): 36-53.
- 879 Reimer, P.J., Austin, W.E., Bard, E., Bayliss, A., Blackwell, P.G., Ramsey, C.B., Butzin, M.,
880 Cheng, H., Edwards, R.L., Friedrich, M. and Grootes, P.M. (2020). The IntCal20 Northern
881 Hemisphere radiocarbon age calibration curve (0–55 cal kBP). *Radiocarbon*, 62(4),
882 pp.725-757.
- 883 Reynolds, R.M. (1993). Physical Oceanography of the Persian Gulf, Strait of Hormuz, and the
884 Gulf of Oman — Results from the Mt. Mitchell Expedition. *Marine Pollution Bulletin* 27:
885 35-59.
- 886 Rimbu, N., Lohmann, G., Lorenz, S.J., Kim, J.H. and Schneider, R.R. (2004). Holocene climate
887 variability as derived from alkenone sea surface temperature and coupled ocean-
888 atmosphere model experiments. *Climate Dynamics*, 23(2), 215-227.
- 889 Safarkhani, E., Yarahmadi, D., Hamzeh, M.A., and Sharafi, S. (2021). Reconstruction of the
890 Persian Gulf SST variability over the last five millennia. *Quaternary International*. Doi:
891 10.1016/j.quaint.2021.01.028
- 892 Saher, M.H., Jung, S.J.A., Elderfield, H., Greaves, M.J. and Kroon, D. (2007). Sea surface
893 temperatures of the western Arabian Sea during the last deglaciation. *Paleoceanography*
894 22 .
- 895 Saidova, K.M. (2010). Benthic foraminifer communities of the Persian Gulf. *Oceanology* 50:
896 61–66.
- 897 Saleh, A., Abtahi, A., Mirzaei, N., Chen, A., Ershadifar, H., Ghaemi, M., Hamzhepour, A.,
898 Abedi, E. (in press). Hypoxia in the Persian Gulf and the Strait of Hormuz. *Marine
899 Pollution Bulletin*.

- 900 Salvatori, S. and Vidale, M. (1982). A brief surface survey of the Protohistoric site of Shahdad
901 (Kerman, Iran): *Rivista di Archeologia* VI 6: 5–10.
- 902 Sarnthein, M. (1972). Sediments and history of the postglacial transgression in the Persian Gulf
903 and northwest Gulf of Oman. *Marine geology*, 12(4): 245-266.
- 904 Schönfeld, J. (1997). The impact of the Mediterranean Outflow Water (MOW) on benthic
905 foraminiferal assemblages and surface sediments at the southern Portuguese continental
906 margin. *Marine Micropaleontology* 29: 211–236.
- 907 Schönfeld, J. (2002a). Recent benthic foraminiferal assemblages in deep high-energy
908 environments from the Gulf of Cadiz (Spain). *Micropaleontology* 44: 141–162.
- 909 Schönfeld, J. (2002b). A new benthic foraminiferal proxy for near-bottom current velocities in
910 the Gulf of Cadiz, northeastern Atlantic Ocean. *Deep-Sea Research I*, 49: 1853–1875.
- 911 Sen Gupta, B. K., Smith, L. E., & Lobegier, M. K. (2006). Attachment of Foraminifera to
912 vestimentiferan tubeworms at cold seeps Refuge from sea-floor hypoxia and sulfide
913 toxicity. *Marine Micropaleontology* 62(1): 1–6.
- 914 Sheppard, C., Al-Husiani, M., Al-Jamali, F., Al-Yamani, F., Baldwin, R., Bishop, J., Benzoni,
915 F., Dutrieux, E., Dulvy, N.K., Durvasula, S.R.V. and Jones, D.A. (2010). The Gulf: a
916 young sea in decline. *Marine Pollution Bulletin* 60(1): 13-38.
- 917 Shimmiel, G., Derrick, S., Mackensen, A., Grobe, H., & Pudsey, C. (1994). The history of
918 barium, biogenic silica and organic carbon accumulation in the Weddell Sea and Antarctic
919 Ocean over the last 150,000 years. In: R. Zahn, T. F. Pedersen, M. A. Kaminski & L.
920 Labeyrie (Eds), *Carbon cycling in the glacial ocean: Constraints on the ocean's role in*
921 *global change* (pp. 555–574). Springer Verlag.
- 922 Sirocko, F., Sarnthein, M., Erlenkeuser, H., Lange, H., Arnold, M., Duplessy, J.C. (1993).
923 Century-scale events in monsoonal climate over the past 24,000 years. *Nature* 364, 322–
924 324.
- 925 Southon, J., Kashgarian, M., Fontugne, M., Metivier, B. and Yim, W.W. (2002) Marine
926 reservoir corrections for the Indian Ocean and Southeast Asia. *Radiocarbon* 44(1), 167-
927 180.
- 928 Taghipour, S., and Taghipour, B. (2009). Mineralogical studies of metasomatic minerals within
929 volcanic rocks of High Zagros salt domes. *Iranian Journal of Crystallography and*
930 *Mineralogy* 4(17): 535-550.
- 931 Tosi, M. (1983). *Prehistoric Sistan: Reports and Memoirs*, v. 19, IsMEO, Rome.
- 932 Vaezi, A., Ghazban, F., Tavakoli, V., Routh, J., Beni, A.N., Bianchi, T.S., Curtis, J.H. and
933 Kylin, H. (2019). A Late Pleistocene-Holocene multi-proxy record of climate variability

934 in the Jazmurian playa, southeastern Iran. *Palaeogeography, Palaeoclimatology,*
935 *Palaeoecology* 514: 754-767.

936 Wick, L., Lemcke, G. and Sturm, M. (2003). Evidence of Lateglacial and Holocene climatic
937 change and human impact in eastern Anatolia: high-resolution pollen, charcoal, isotopic
938 and geochemical records from the laminated sediments of Lake Van, Turkey. *The*
939 *Holocene* 13(5): 665-675.

940 Wyrтки, K. 1971. Oceanographic atlas of the International Indian Ocean Expedition. Nat. Sci.
941 Found. Washington D.C., 531 p.

942 Yao, F., and Johns, W.E. (2010). A HYCOM modeling study of the Persian Gulf: 2. Formation
943 and export of Persian Gulf Water. *Journal of Geophysical Research: Oceans* 115(C11).

944 Zhong, Y., Chen, Z., Li, L., Liu, J., Li, G., Zheng, X., Wang, S. and Mo, A. (2017). Bottom
945 water hydrodynamic provinces and transport patterns of the northern South China Sea:
946 Evidence from grain size of the terrigenous sediments. *Continental Shelf Research* 140:
947 11-26.

948

949

950

951

952

953

954

955

956

957

958

959

960

961

962

963 **Appendices**

964 A1: List of benthic foraminiferal taxa (order, family genus and species) identified from the core T2S3

Order	Family	Genus	Species
Astrorhizida	Rhabdamminidae	<i>Marsipella</i>	sp1
Lagenida	Lagenidae	<i>Lagena</i>	<i>perlucida, semistriata</i>
	Ellipsolagenidae	<i>Fissurina</i>	<i>bispinata, lucida</i>
		<i>Oolina</i>	sp1
	Nodosariidae	<i>Pyramidulina</i>	sp1
Lituolida	Trochamminidae	<i>Trochammina</i>	sp1, sp2
Miliolida	Cribrolinoididae	<i>Adelosina</i>	<i>honghensis, laevigata</i>
	Hauerinidae	<i>Quinqueloculina</i>	<i>bosciana, limbata, quinquecarinata, seminula, sp5, sp6, sp7, sp8, sp9</i>
		<i>Sigmoilopsis</i>	sp1, sp2
		<i>Triloculina</i>	<i>tricarinata, trigonula, wiesneri</i>
	Ophthalmidiidae	<i>Spirophthalmidium</i>	sp1
	Spiroloculinidae	<i>Spiroloculina</i>	<i>communis, depressa, elegantissima</i>
Clornuspiridae	<i>Cornuspira</i>	<i>involvens</i>	
Rotaliida	Ammoniididae	<i>Ammonia</i>	<i>beccarii, tepida, faceta, sp4</i>
		<i>Asterorotalia</i>	<i>dentata, milletti</i>
		<i>Challengerella</i>	<i>Bradyi</i>
	Anomalinidae	<i>Hanzawaia</i>	<i>leroyi, tagaensis</i>
	Bolivinitidae	<i>Bolivina</i>	<i>dilatata, dottiana, foxenensis, spathulata, striatula, translucens, sp7, sp8.</i>
		<i>Fursenkoina</i>	sp1
	Buliminidae	<i>Bulimina</i>	<i>Marginate, sp2</i>
	Cancrisidae	<i>Cancris</i>	<i>oblongus, auriculus</i>
	Cassidulinidae	<i>Cassidulina</i>	<i>laevigata</i>
	Cibicididae	<i>Cibicides</i>	<i>lobatulus</i>
	Elphidiidae	<i>Criboelphidium</i>	<i>excavatum</i>
		<i>Elphidium</i>	<i>advenum, fichtellianum, hispidulum.</i>
	Globorotaliidae	<i>Globorotalia</i>	sp1
	Nonionidae	<i>Nonion</i>	sp1, sp2, sp3
	Planorbulinidae	<i>Hyalinea</i>	sp1
	Rosalinidae	<i>Rosalina</i>	sp1
Trimosinidae	<i>Trimosina</i>	sp1	
Textulariida	Textulariidae	<i>Textularia</i>	<i>bocki, conica, earlandi, foliacea, sp5, sp6</i>

965

Highlights:

- During the last 5000 years, PGDW intensity has been under influence of the continental climate of SW Asia and the Arabian Sea SST.
- During the periods of increased SST (4500 to 3000 and 1400 cal yr BP to present), bottom current energy of the Strait of Hormoz increased and a notable decrease occurred in river discharges.
- Although high energy bottom currents provide a hostile environment for the benthic fauna, it causes domination of suspension feeder epifaunal foraminifera by carrying high DO content bottom waters.

Declaration of interests

The authors declare that they have no known competing financial interests or personal relationships that could have appeared to influence the work reported in this paper.

Journal Pre-proof